Graphene Nanoparticle-Polymer Composite Fabricated by Pulsed Laser Ablation in Liquid

by

Mervat Alamri

A thesis
presented to the University of Waterloo
in fulfillment of the
thesis requirement for the degree of
Master of Applied Science
in
Systems Design Engineering (Nanotechnology)

Waterloo, Ontario, Canada, 2016

AUTHOR'S DECLARATION

I hereby declare that I am the sole author of this thesis. This is a true copy of the thesis, including any required final revisions, as accepted by my examiners.

I understand that my thesis may be made electronically available to the public.

Abstract

Graphene is an attractive alternative material for diverse applications in electronic devices, fuel cells, biomedical sensors, energy storage, and super-capacitors due to its exceptional thermal, electrical, optical and mechanical properties. This material can be synthesized by many effective methods such as chemical vapor deposition (CVD), micromechanical exfoliation of graphite, and reduction of graphene oxide. Each of these methods has its advantages and disadvantages.

This thesis investigates a novel and clean approach to grow graphene directly from bulk graphite by Pulsed Laser Ablation in Liquid, whereas the graphite sheets are immersed in different polymeric solutions (deionized Water, Ethanol, and Toluene) and exposed to two types of lasers (nanosecond and femtosecond lasers). This technique is simple, and fast; a one-step procedure to fabricate pure and stable graphene nanoparticles (GNPs) by short ablation time. It results in controllable-size products, high mass production, high stability, less aggregation, and absence of chemical agents, a known disadvantage observed in other approaches for graphene production.

The ablation parameters had been optimized for the best formation efficiency of Pulsed Laser Ablation in Liquid (PLAL) process, after controllably varied trials, which are: 532 nm and 800 nm λ - wavelength for the nanosecond laser and femtosecond laser respectively, with pulse width of 150 ns for ns-laser and 35 fs for fs-laser. The pulse energy are 800 μJ and 250 μJ for the ns-laser and fs-laser respectively, 1kHz is the repetition rate for both lasers. Ablation times are 20 minutes for ns-laser and 1-2 hours for fs-laser, and 5 cm focal length for the focusing lens.

Confirming the presence of graphene in solutions or in fabricated thin films is carried out by several characterization techniques including Raman; UV-VISIBLE; atomic force microscopy (AFM); scanning electron microscope (SEM); and transmission electron microscopy (TEM).

These techniques allow an insight into the morphological and structural properties of the produced graphene, confirming the purity; particle size uniformity; as well as the number of graphene layers.

This thesis attempts to interpret three main aspects of graphene growth: the advantages of the use of the PLAL approach and how it overcomes some of the reported challenges in graphene growth processes; the function of the contribution of different polymers which enhances the formation efficiency, and prevents agglomeration of carbon-based materials of the prepared GNP. Finally, the potential recipe that had been used for growing high quality graphene, with controllable thickness and particle size, was employed in the results section of this thesis.

Acknowledgements

First and foremost, I must acknowledge the support and guidance of my Supervisors, Dr. Eihab Abdel-Rahman, Dr. Mustafa Yavuz, and Dr. Andrew Brzezinski. Without their dedicated efforts, this work would not have been achieved. I must also acknowledge the continual efforts of Dr. Mehrdad Irannejad, the research associate in our group, towards aiding me to overcome the laboratory concerns and limiting the technical issues. Also I acknowledge Dr. Baris Fidan for being one of the reader committee of my thesis.

I would also like to acknowledge Dr. Homeira Faramarzi, the previous research associate in our group, for helping me to set up the laser's parameters at the laser workstation in the Physics lab. Also I acknowledge my friend, Wadha Alyalak, who has helped me challenge the conventional concerns during my training for AFM and Raman spectroscopy at Giga-to-Nano lab. I must also acknowledge my colleague, Salamt, who has been very supportive and helpful; he never hesitated to answer my scientific questions even by email with very short notice. His valuable explanation and interest in answering all my questions is a testament to his dedication.

I cannot express my gratitude and appreciation for the love and support that my parents, Fatemah Alamri and Safar Alamri, have dedicated towards enabling me to pursue my dreams in any path of my choosing. Without their tireless efforts, I would never be where I am now. The same appreciation extends to my dear sister, Nada, for her tremendous support emotionally and financially all the way; also to my brothers Abdel-Wahab, Haytham, Ali, and Mazen who remain aware of all the challenges I faced and always supportive. I wholeheartedly thank all of them for being always engaged.

I must also acknowledge my friend, Amal Alshehri, for her unwavering love and constant attention and support. Her encouraging sayings and lovely prayers helped me to overcome the difficult feeling of homesickness and kept my motivation levels high whenever I was overwhelmed. Special acknowledgment goes to my most ambitious friend, Dr. Aisha Alamri, for her encouragement throughout my journey to study abroad.

I own my deepest thanks to Eng. Meshael Alqahtani for her outstanding patience, spirit and dedication in supporting me throughout the writing of this thesis. Her guidance was indispensable since she is an alumnus of Systems Design Engineering at the University of Waterloo.

Finally, I thank the late Saudi king, King Abdel-Allah, *may Allah have mercy on him*, for offering me the greatest opportunity ever of a fully guaranteed scholarship, which has enabled me to undertake my higher education. Also, the continuous assistance from the Saudi Arabian Cultural Bureau in Canada is also gratefully acknowledged, with special appreciation for both supervisors, Dr. Mohamad Najem and Dr. Yousef Abu-Nada, for their great supervision and help for all UW Saudi students including myself.

Dedication

I dedicate this thesis to my parents and to my brother, Haytham.

Your support has enabled me to study at the university of my dream.

Table of Contents

List of Figures

List of Tables

Chapter 1: Introduction

1.1 Graphene synthesis

Graphene is a flat monolayer of carbon atoms tightly attached and packed into a two-dimensional (2D) hexagonal structure [1] with a carbon–carbon bond length of 0.142 nm. [2] It can be wrapped up into 0 dimension fullerenes, rolled into 1 dimension nanotubes or stacked into 3 dimensions as graphite [3] as shown in Figure 1-1. The exceptional thermal, electrical, mechanical, and optical properties [4] of graphene make it an attractive material for diverse applications in electronic devices, fuel cells, and sensors. [1], [5]

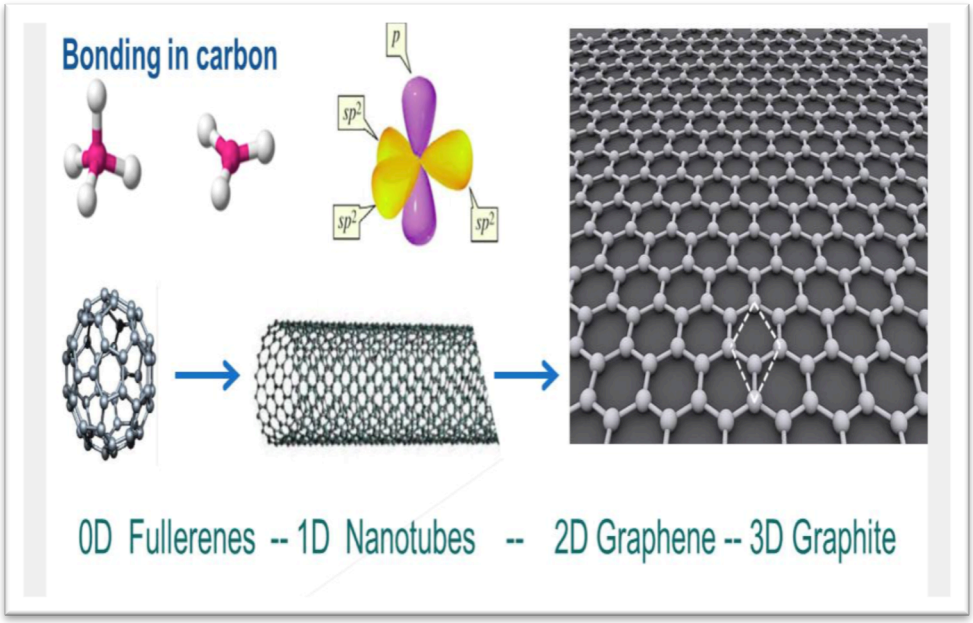

Figure 1-1: Graphene in different forms; a.) Wrapped up into 0 dimension fullerenes, b.) rolled into 1 dimensional nanotubes, and c.) Stacked into 3-dimensional graphite.

Although graphite was discovered and has been used 6000 years ago; research on graphene dates back to the 1940s [6] 1960s. [2] Sixty years later, a couple of high-quality sheets of micrometer-sized graphene flakes were obtained. [6] Moreover, scientists were looking for graphene using complex experiments until 2004, when Geim

and Novoselov, attempting to make a transistor using one layer of graphite, were able to obtain the first crystal of graphene as a transferable material [7] as shown in Figure 1-2 . Interestingly enough, the graphene was isolated from graphite by micromechanical cleavage using an "ordinary scotch tape" which is a very simple, yet effective, method that resulted in high-quality crystallites over 100 μm^2 in size. [7] The two physicists, Geim and Novoselov, were awarded a Nobel Prize in 2010 in physics for their simple but groundbreaking experiment. [2], [7]

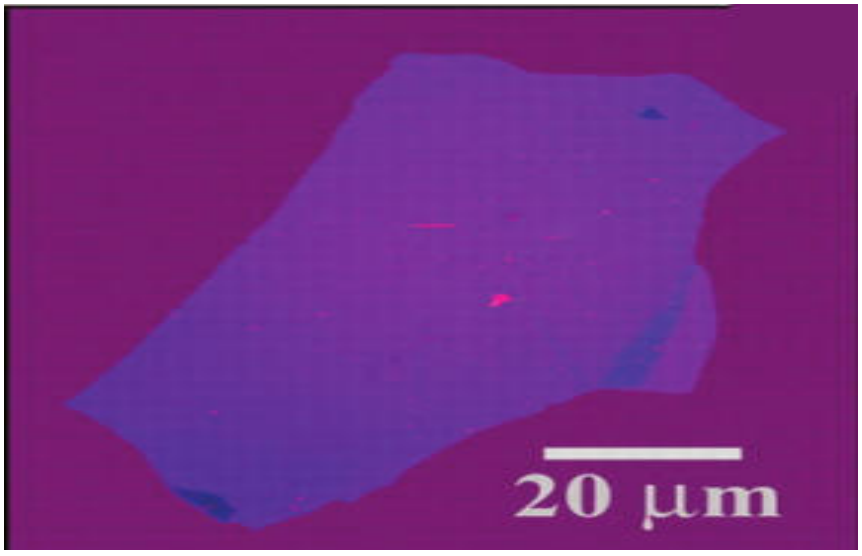

Figure 1-2: Geim and others first observed single layer graphene at Manchester University. Here a few layer flakes are shown, with optical contrast enhanced by an interference effect at a carefully chosen thickness of oxide. [7]

Since then, developing routes for obtaining graphene-nanoparticle hybrids and large sheets of monolayer or bilayer graphene has been a goal of enormous importance all over the world. [7] The following graph in Figure 1-3 presents the numbers of publications on graphene-nanoparticle hybrids from 2004 to 2013 according to Scopus.

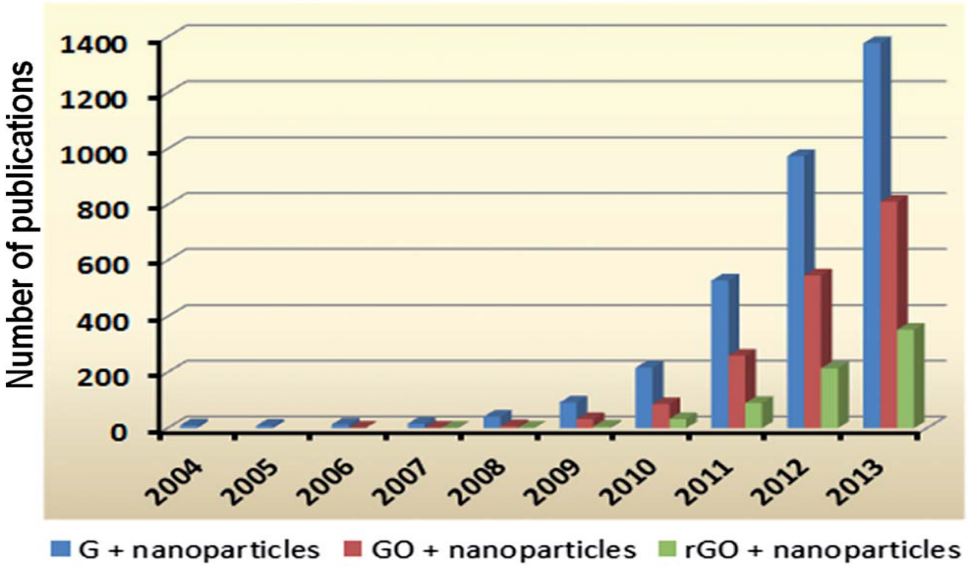

Figure 1-3: The numbers of articles published on graphene-nanoparticle hybrids from 2004 to 2013 according to Scopus. Adapted from. [8]

1.1.1 Graphene properties

Graphene is the strongest known material in the universe due to the strength of its 0.142nm long carbon bonds with a 130 GPa tensile strength. [9] It has an excellent thermal conductivity (3000–5000 W m^{1} K^{1}) at room temperature [10], ten times higher than copper [6], Additionally, graphene has the highest carrier mobility of more than 200,000 cm^2/ (V· s) [11] and electron mobility: 10,000-15,000 cm^2/(V s) for exfoliated graphene on SiO_2 substrate and larger than 3,700 cm^2/(V s) for large-scale graphene. These electron mobility and motility measurements are for graphene that has been grown on nickel followed by a transferring process to different substrates such as Si. [12] Simply, the electron mobility of graphene is about 100 times higher than silicon. [6] Furthermore, graphene has other important features, such as excellent optical transparency (≈ 97.3%) and extraordinary mechanical strength with a Young's modulus of 1.0 TPa, which strongly contributes to making graphene a "wonder material". [9]

1.1.2 Potential applications of graphene

Graphene has become a very attractive alternative material in different areas including but not limited to: graphene-based biosensors for small biomolecules and other biomedical implementations, energy storage, fuel cells and super-capacitors, as well as limitless use in optical electronics for computing and smart screen applications. Moreover; being a transparent conductor is a very important feature of graphene, which may have a very significant impact on the solar industry. [7] Two examples for graphene's high efficiency promise will be fundamentally explained in the following: optical electronics and ultrafiltration

1.1.2.1 Optical Electronics

As promised by scientists all over the world, graphene will improve the efficiency and performance of current devices in various fields. [1] Therefore, graphene must be a preferred material over currently existing materials that are industrially available such as indium tin oxide (ITO). [4] Hence, there are precise properties for any material utilized in optoelectronics such as tablets, LCD desktop computers, and smart screens. These properties include low electrical resistance, and most importantly, the high transmission rate of light of approximately 97%. Also, the possibility to adjust the Fermi level [13] leads to changing the optical absorption of graphene, which is an important property for advanced optoelectronics technology. The most well-known material that has been widely used and performs very well in optoelectronics is Indium tin oxide (ITO). [13] Nevertheless, the outstanding properties possessed by graphene would make it a suitable replacement of ITO as it potentially matches with the properties of current high standards ITO. [14], [5], [13] For instance, an outstanding property of graphene is the graphene transparency, which is 97.3% per monolayer, which greatly meets the standard demand. [13]

1.1.2.2 Ultrafiltration

Ultrafiltration application requires a material that is as strong and thin as much as possible. As mentioned earlier in this thesis, the extraordinary properties of the 2-dimensional graphene and its derivatives are intended to make a significant improvement in the ultrafiltration field. This improvement relies on the thickness, while graphene is only an atom thick; the smallness of the nano graphene molecules will not allow any gases such as Helium molecules [6] or other impurities to pass through the filters. Also, when a layer of graphene is employed as a filter, this layer will act as a barrier, which can measure the strain and pressure between the substances electronically. [16] [17]

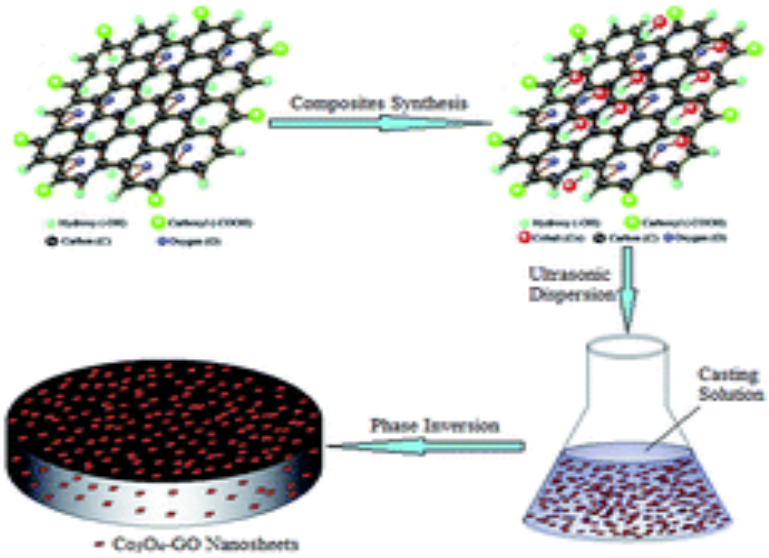

Figure 1-4: The process scheme of preparation of hybrid ultrafiltration membrane. [15]

1.2 Graphene vs. Graphite:

To understand the origin of the graphene material, different allotropes of carbon should be demonstrated; thus, the following covers the fundamental structures of each form of the carbon element.

1.2.1 Carbon Allotropes

Natural elements can be found in different physical forms in nature and these are known as allotropes. Intrinsically, the atomic arrangements in an element within their bulk structure are responsible for making different allotrope forms. In the case of carbon, specifically in diamond and graphite, atoms produce giant macromolecular structures, which happens when all of the atoms in the bulk structure are joined together by covalent bonds.

1.2.2 Diamond structure

In a diamond crystal, each carbon is bonded to four other carbon atoms making a giant macromolecular array (lattice) as shown in Figure 1-5. Each carbon has tetrahedral bond angles of 109º 28' and four single bonds sp^3 hybridized.

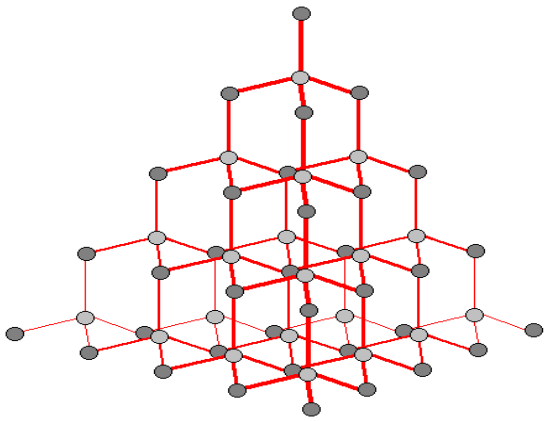

Figure 1-5: The diamond structure.

1.2.3 Graphite structure

The classical graphite consists of many sheets of hexagonal rings forming thin parallel plates. Each carbon atom is linked by covalent bond to three other atoms in the plate, the angle between two bonds is 120° as it is schematically shown in Figure 1-6. The outer shell of a carbon atom has four valence electrons; three of them are used to form the covalent bonds. Consequently, the forth-free electron is delocalized and does not take part in covalent bonds, which can easily be displaced from the electron shell and conduct electricity and heat when

applying electric field. These electrons provide the electrical conductivity of graphite. Therefore, the graphene atoms are bonded to each other by weak Van der Waals forces. The layered structure of graphite allows a sliding movement of the parallel graphene plates. As such, the weak bonding between the layers is the reason behind the softness property of graphite and makes it an excellent lubricant. In other words, graphite can be viewed as a stack of graphene layers as Figure 1-7 shows. [18], [19]

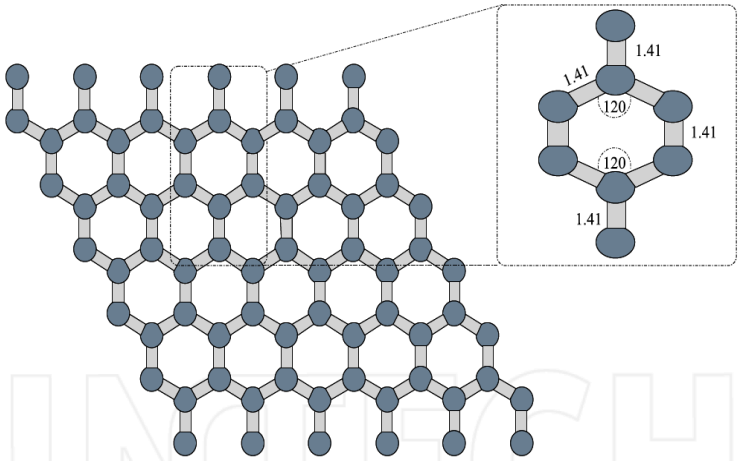

Figure 1-6: The angle between the graphite layers is 120 °, C-C-C bond - adapted from. [19]

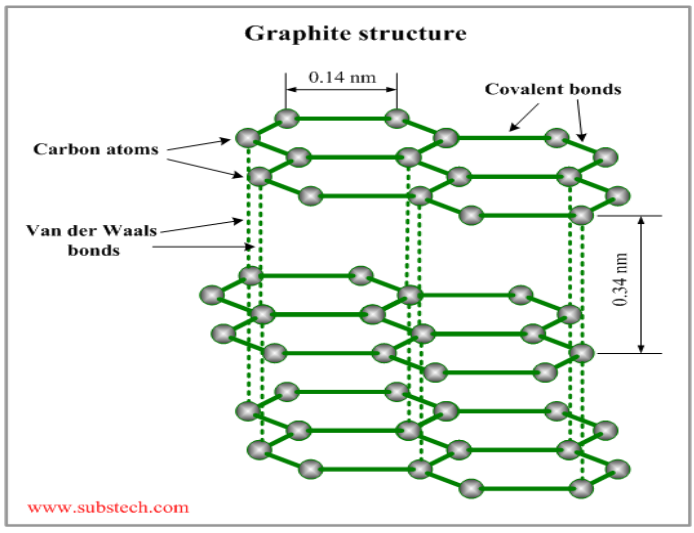

Figure 1-7: Graphite structure viewed as a stack of graphene layers.

1.2.4 Graphene structure

Graphene fundamentally is one single layer of graphite; a layer of sp2 bonded carbon atoms arranged in a honeycomb (hexagonal) lattice as Figure 1-8 shows. Essentially it is the basic structural unit of some of the carbon allotropes, including graphite, carbon nanotubes and fullerenes. [18], [19]

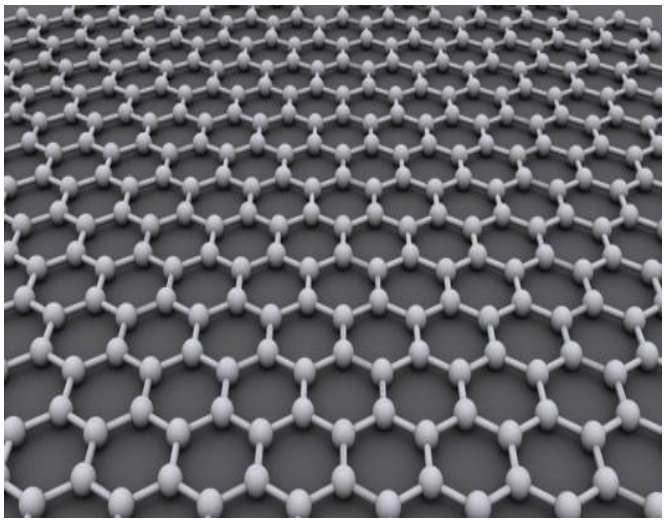

Figure 1-8: Schematic structure of graphene.

1.3 Graphene bonds

In graphene structure, each hybridized carbon consists of three atomic orbitals: s, px, and py which are responsible in forming strong covalent sp^2 bonds, resulting in 120 ° C-C-C bond angles between graphite layers . The band of empty π^* orbitals is known as the conduction band and the band of filled π orbitals is known as the valence band. In the graphene when the remaining pz orbital of each carbon overlaps with its three neighboring carbons lattice, both bands π^* and π are formed. The σ (single) bonds in graphite are formed by three of the four valence electrons of each carbon. The carbon-carbon bond in graphite is formed by the fourth of the valence electrons. [7]

1.4 Polymeric graphene

Integrating graphene as nanofillers in the material fabrication process improves upon other classical nanofillers such as (Na-MMT, LDH, CNT, CNF, EG, etc.) that are due to its intrinsic properties such as high surface area aspect ratio, EMI shielding ability, flexibility, and low coefficient of thermal expansion CTE. The following comparative chart confirms the excellent mechanical, thermal and electrical properties of graphene as compared to CNT, steel, rubber, plastic, and fiber as the following Table 1-1 shows. Moreover, "It was also reported that the improvement in mechanical and electrical properties of graphene based polymer nanocomposites are much better in comparison to that of clay or other carbon filler-based polymer nanocomposites as Table 1-2 shows"; "the improvement in the physicochemical properties of the nanocomposites depends on the distribution of graphene layers in the polymer matrix as well as interfacial bonding between the graphene layers and polymer matrix". [1]

Table 1-1: Properties of graphene, CNT, nano sized steel, and polymers. [1]

Materials	Tensile strength	Thermal conductivity (W/mk) at room temperature	Electrical conductivity (S/m)	References
Graphene	130 ± 10 GPa	$(4.84 \pm 0.44) \times 10^3$ to $(5.30 \pm 0.48) \times 10^3$	7200	[73–84]
CNT	60–150 GPa	3500	3000–4000	[35,85–88]
Nano sized steel	1769 MPa	5–6	1.35×10^6	[89,90]
Plastic (HDPE)	18–20 MPa	0.46–0.52	Insulator	[91–93]
Rubber (natural rubber)	20–30	0.13–0.142	Insulator	[94,95]
Fiber (Kevlar)	3620 MPa	0.04	Insulator	[96,97]

Table 1-2: Electrical properties of graphene/graphite based polymer nanocomposites. [1]

Matrix	Filler type	Filler loading (wt.%[a], vol.%[b])	Process	% Increase E	% Increase TS	% Increase flexural strength	Reference
Epoxy	EG	1[a]	Sonication	8	−20		[149]
	EG	1[a]	Shear	11	−7		[149]
	EG	1[a]	Sonication and shear	15	−6		[149]
	EG	0.1[a]	Solution			87	[30]
PMMA	EG	21[a]	Solution	21			[159]
	GNP	5[a]	Solution	133			[160]
PP	EG	3[b]	Melt			8	[165]
	xGnP-1	3[b]	Melt			26	[166]
	xGnP-15	3[b]	Melt			8	[166]
	Graphite	2.5[b]	SSSP		60		[168]
LLDPE	xGnP	15[a]	Solution		200		[172]
	Parrafin coated xGnP	30	Solution		22		[173]
HDPE	EG	3[a]	Melt	100	4		[175]
	UG	3[a]	Melt	33			[175]
PPS	EG	4[a]	Melt			−20	[182]
	S-EG	4[a]	Melt			−33	[182]
PVA	GO	0.7[a]	Solution		76		[73]
	Graphene	1.8[b]	Solution		150		[195]
TPU	Graphene	5.1[b]	Solution	200			[46]
	Sulfonated Graphene	1[a]	Solution		75		[100]
PETI	EG	5[a]	*In situ*	39			[192]
		10[a]	*In situ*	42			[193]

1.5 Graphene nanoparticles

Nanomaterials consist of structural elements such as particles, grains, crystallites, fibres, rods, and layers with dimensions of several nanometers to several tens of nanometers. The importance of determining the arrangement of structural elements either by the size of the molecule or mutual arrangement allows for the demonstration of all macroscopic properties of the examined material.

Nanocrystalline material including graphene and its derivatives, are commonly categorized based on the dimensions of their structural elements: zero-dimensional (0D), one-dimensional (1D), two-dimensional (2D), and three-dimensional (3D) as Figure 1-9 shows.

Materials in which nanoparticles are isolated from each other are an example of zero-dimensional nanomaterials that include nanocluster materials and nanodispersions. Nanofibre (nanorod) and nanotubular materials with fibre (rod, tube) are examples of one-dimensional nanomaterials with lengths from 100 nm to tens of microns, whereas the 2D-nanomaterials are films with nanometer thickness in which the use of coatings is an essential step of the preparation process.

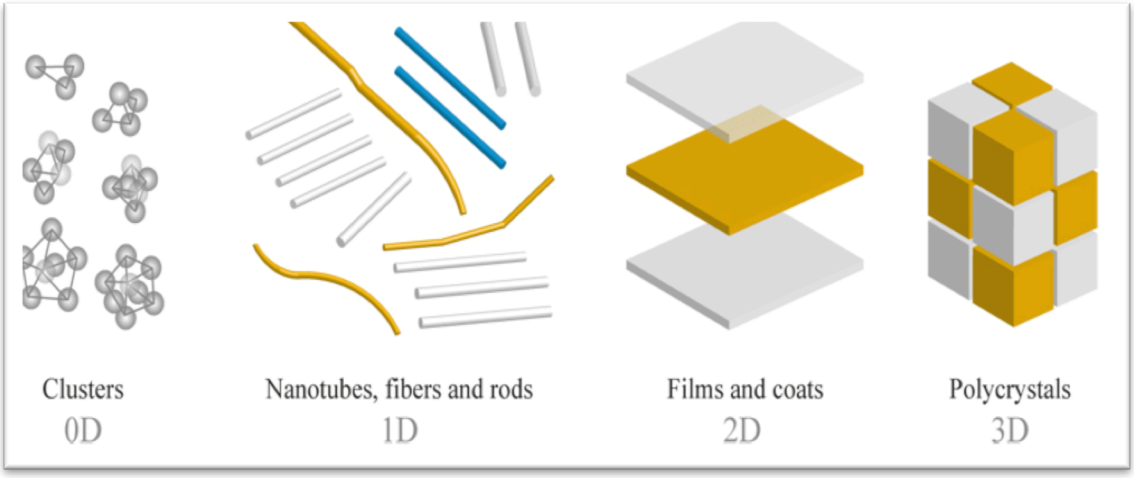

Figure 1-9: Types of nanocrystalline materials by size of their structural elements: clusters are 0D (zero-dimensional); nanotubes, fibers and rods are1D (one-dimensional); films and coats are 2D (two-dimensional); polycrystals are 3D (three-dimensional). [18]

In 0D, 1D and 2D nanomaterials, the structural elements can be distributed in a liquid or solid macroscopic matrix or be applied on a substrate. A compact or consolidated (bulk) polycrystal with nanosize grains is an important type of three-dimensional nanostructured material and these include powders, fibres whose entire volume is filled with these nanograins, and the absence of free surface of the grains results in only grain interfaces. Thus, the fundamental difference between 3D-nanomaterials and nanocrystalline powders is the formation of grain interfaces and the "absence" of the nanoparticle (nanograin) surface with different degrees of agglomeration in particles with the same size as the compact nanostructured materials. [18]

1.6 Laser ablation and nanoparticle fabrication

PLAL (Pulsed Laser Ablation in Liquid) is already a well-established technique in research and has become a considerably interesting approach to generate micro/nanostructure directly from bulk material particularly in photochemistry and physical chemistry areas. The ability to synthesize nanoparticles of various materials, with the desired sizes and shapes, as well as to assemble them effectively for certain applications is the researches' essential motivation in the field of nanotechnology. In the present work, PLAL technique holds great potential for the well-controlled synthesis of graphene [20], as will be discussed in Chapter 3.

1.7 Thesis overview

The first chapter covered graphene synthesis, properties, roots, and polymeric graphene alongside a brief introduction about the major goal of this thesis, which is to produce graphene nanostructure via Laser Ablation technique in a liquid environment. This will be followed by a discussion of graphene nanoparticle fabrication and characterization processes in the following chapters of this thesis.

In overview, graphene nanostructures including flakes, particles, and quantum dots were prepared by pulsed laser ablation of a graphite target immersed in deionized water or aqueous solutions of water with PVA- Polyvinyl alcohol, ethanol with PMMA- Poly (methyl methacrylate), as well as Toluene with PS- Polystyrene. The structures, morphologies, and compositions of the resultant GNP-graphene nanoparticles were investigated by UV-visible, atomic force microscopic (AFM), scanning electron microscope (SEM), and transmission electron microscopy (TEM).

This thesis attempts to build a possible formation mechanism of graphene nanostructural growth. In the first half of this thesis, the laser ablation process is theoretically analyzed. Then, the typical materials that have been investigated by PLAL are summarized. Finally, the potential recipe of fabricating complex graphene nanostructures is discussed.

Chapter 2: Graphene nanostructures

2.1 Introduction

Graphene nano-structures can be fabricated by various methods. To name a few: Chemical vapor deposition (CVD), the micromechanical exfoliation of graphite, epitaxial growth, and solution-based reduction of graphene oxide [5] [1], which will be covered below in more detail.

2.2 Techniques used to fabricate graphene nanostructures

Substantially, synthesis of nanostructured materials including graphene can be divided into two main categories:

2.2.1 The top-down approach

Whereby a bulk material is reduced down to nano- scale objects, examples of such approach are mechanical exfoliation and chemical oxidation/exfoliation. [8] An advantage of this class of fabrication is that it offers precise control over the size and shape of the produced material. Nevertheless, a disadvantage is that the point-by-point or layer-by-layer processing makes this approach time-consuming and has a limit for scale up. [8]

2.2.2 The bottom-up approach

Which involves constructing nanostructures one atom or molecular unit at a time by chemical synthesis and unit by unit at a time through self-assembly, examples of the bottom-up approach is epitaxial growth and Chemical vapor deposition (CVD). Simplicity and flexibility are advantages of this approach. In addition, another advantage is that the building blocks can be designed precisely to simplify the assembly of nanostructures with tailorable features. The following Figure 2-1 describes

schematically the differences between the two approaches Top-down and Bottom-up to fabricate carbon-based nanomaterials.

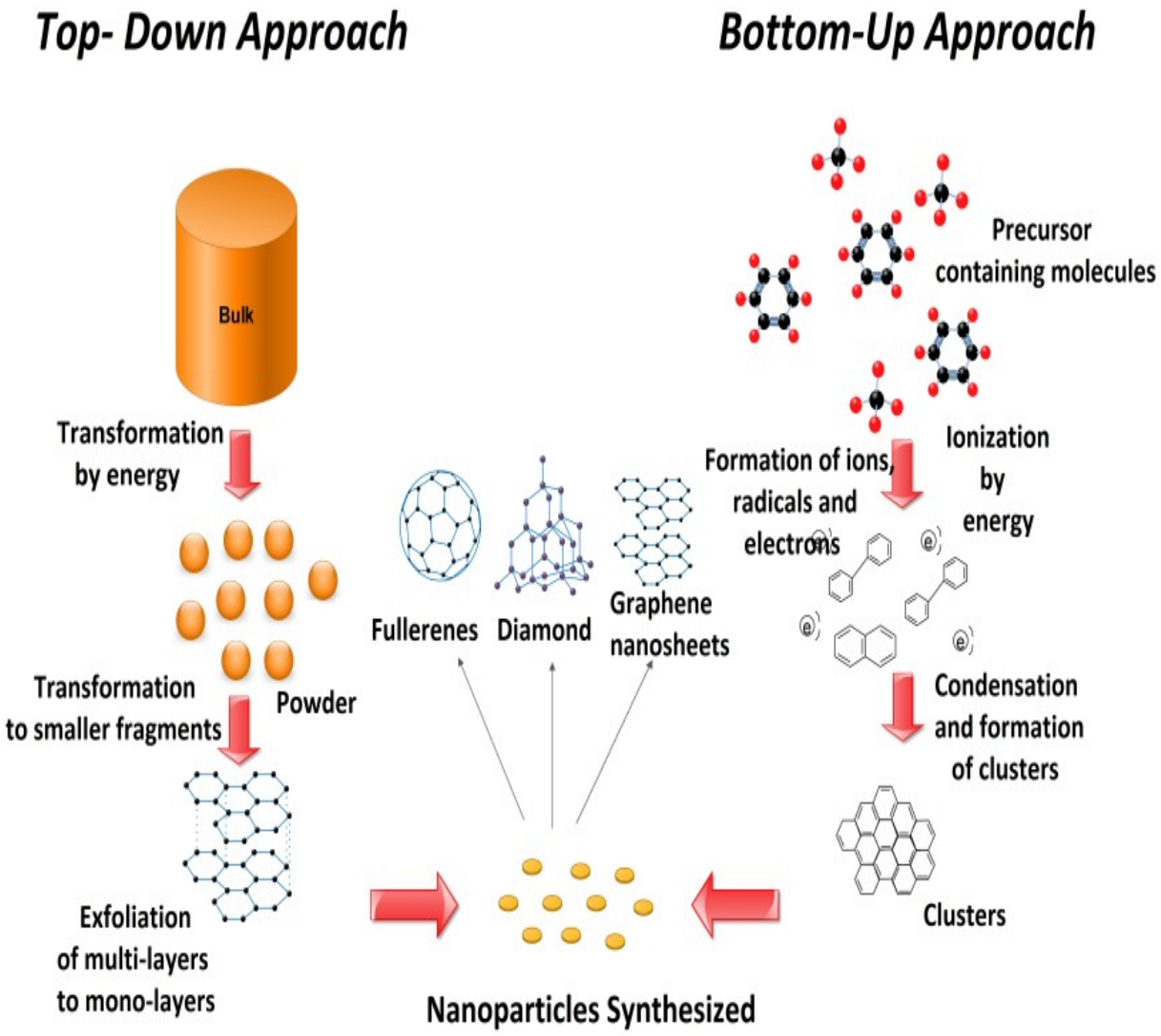

Figure 2-1: Bottom-up and top-down approaches in the synthesis of carbon-based nanomaterials. [21]

Moreover, in terms of techniques to fabricate graphene nanostructure, it is categorized into two main categories based upon the structural morphologies of the final hybrids. Whereas the first

category classified the nanoparticles decorated on graphene or its derivatives, and the second category classified the nanoparticles wrapped by graphene or its derivatives as the below diagram in Figure 2-2 categorize. [8]

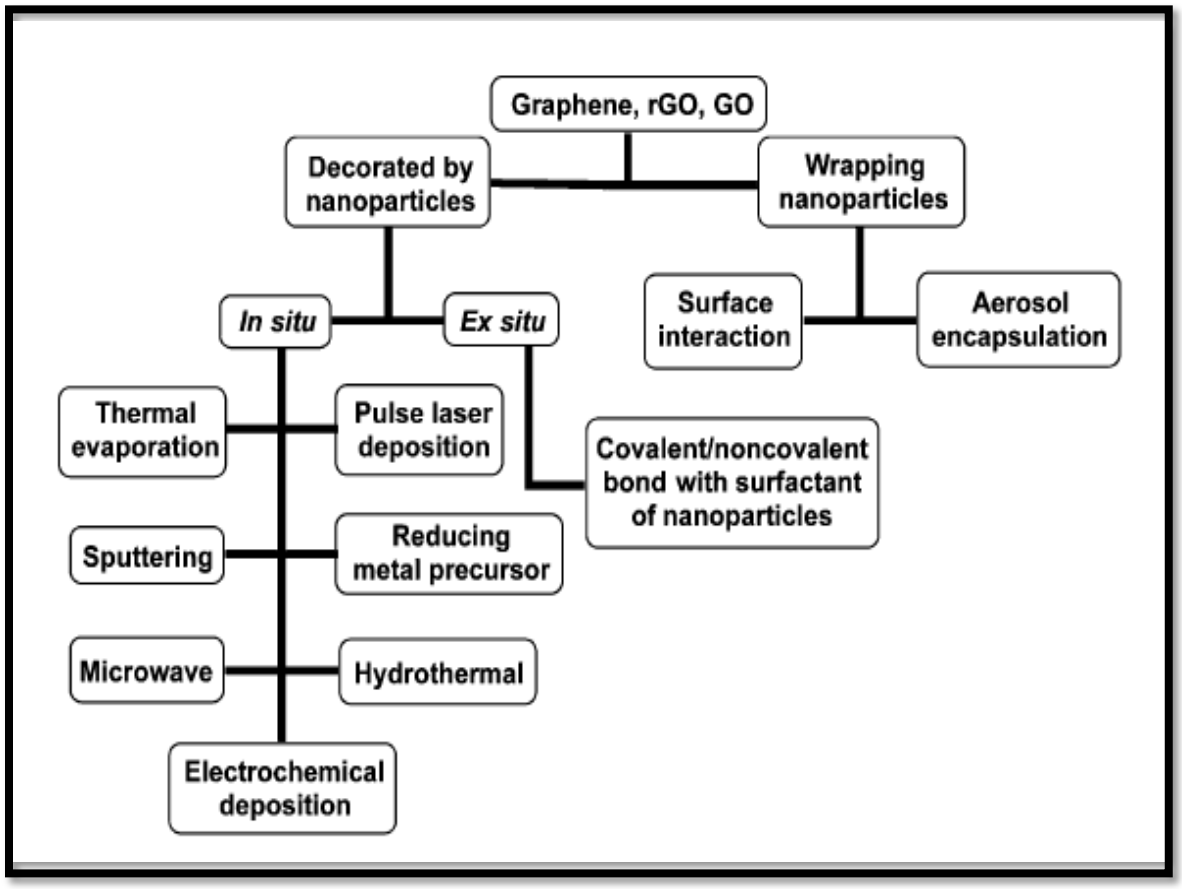

Figure 2-2: Diagram to categorize the techniques to fabricate graphene nanostructure.

2.3 Conclusion

The precise demand for high quality and high yields graphene kept motivating researchers to figure out a simple, clean, yet scalable methods to produce graphene. As this chapter covered, the techniques used to fabricate graphene nanostructures divided into two main categories; the top-down and bottom-up, which consequently consist of different chemical, physical, or mechanical approaches to fabricate graphene.

Chapter 3: Graphene nanoparticle/ polymer composite fabrication by Pulsed Laser Ablation in Liquid

This chapter consists of three sections. The first section presents a brief background about the PLAL technique. The second and the third sections present the methodology that has been used in this research project.

3.1 Introduction

There has been noticeable interest in developing techniques for the fabrication of nanostructures from their bulk material and this has been extensively focused on by all nanotechnology researchers. This is because one of the most challenging factors occurring in this field is the scaling down of the produced material while maintaining the standard qualities for different applications. [22] As aforementioned in this thesis, fabrication techniques are generally categorized into two main approaches, either bottom-up assembly or top-down fabrication. [22] Therefore, laser ablation of solids is considered as a top-down approach [22] and is garnering widespread attention due to the mechanism's simplicity and other positive factors, which will be covered in this chapter.

3.2 History and principle of PLAL

"By definition, laser ablation is the ejection of macroscopic amounts of materials from the surface of a solid usually induced by the interaction of short (∼10−13 to 10−8 s), intense (∼106 to1014 W/cm^2) laser pulses with the surface." [23].

Historically, since the invention of the ruby laser in the 1960s, significant progress has been made in the field of laser ablation, which makes PLAL a viable technique that functions perfectly with all three different states of material: gas, solid, or liquid. The usage of Pulsed laser irradiation was explored by Patil et al. in 1987. They used iron as a target in a water medium and since then the

fabrication possibilities at a liquid–solid interface by pulsed laser irradiation was discovered. Soon after, Neddersen et al. reported the synthesis of colloids by laser ablation of metallic targets in water and organic solvents. Later, in the 2000s, PLAL held a great potential to generate nanostructure materials. More specifically; the synthesis of noble metal nanoparticles (NPs) with a controllable particle size in aqueous solutions of surfactants were achieved by PLAL. [23]

3.3 Experimental setup

Figure 3-1 describes the typical experimental setup of PLAL, which basically requires a pulsed laser, beam delivery optics, and a vessel to hold the target and liquid. Throughout the irradiation process, the vessel and the target should be rotating to avoid a deep ablation crater.

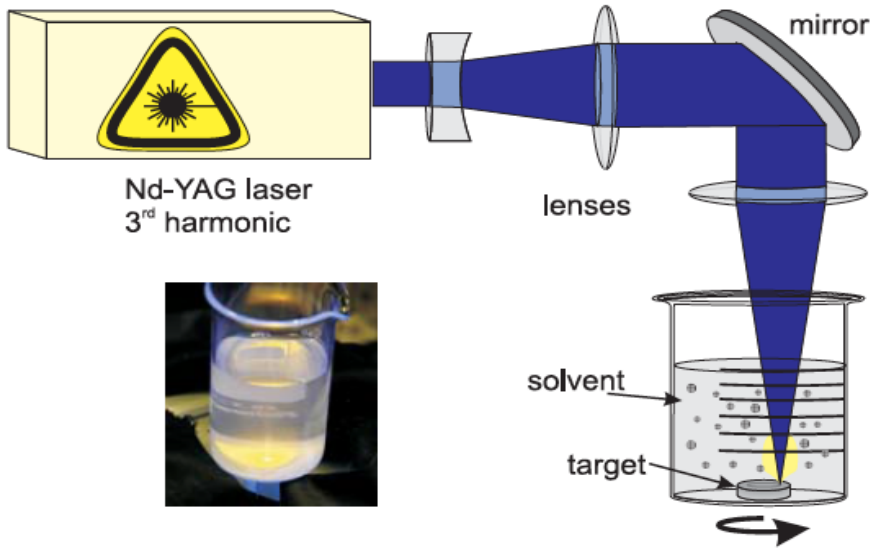

Figure 3-1: Scheme of the PLAL experiment. The laser is focused on the target, which is rotated. Plasma is generated from which the nanoparticles are formed. On the picture, one can see the impact on the target as well as the plasma plume and its luminescence. [24]

The setup could be modified in different ways as long as the most important features still

exist and held the series of interactions as shown schematically Figure 3-2, which are a laser beam focused onto a target immersed in liquid, and the exposed materials are dispersed into the liquid. [23]

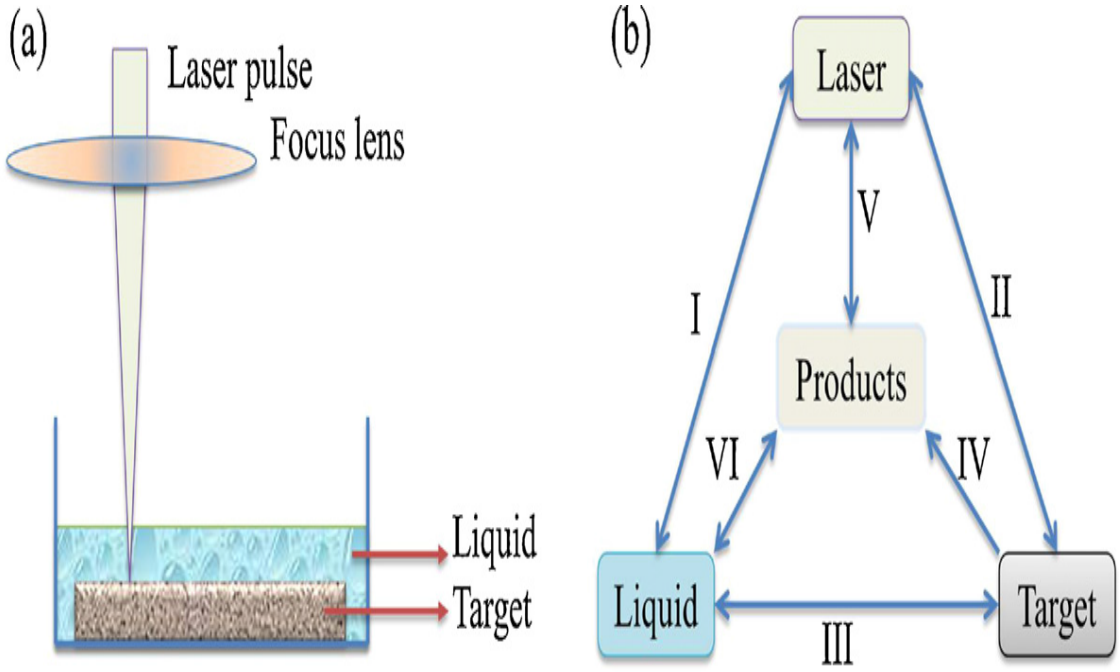

Figure 3-2: (a) Schematic diagram of the experimental setup of PLAL. (b) A combinatorial library of constituents and interactions in PLAL: (I) laser–liquid interaction; (II) laser ablation of the target; (III) liquid–(hot) target interaction; (IV) generation of products from the target; (V) laser–products interaction; (VI) liquid–products interaction. [23]

In principle, when material is exposed to a laser in a vacuum, gaseous or liquid medium, there is either reflection or absorption which occurs for the incident light. Thus, the absorbed energy reacts with the material thermally and/or chemically causes rapid vaporization process and consequently forming plasma on the target. Then, the particles in the diameter of nanometer and micrometer begin to form and gathered in the solution medium. The following images in Figure 3-3 show steps

of the interactions between laser and the surface of the targeted material to form nanometer and micrometer particles. [25]

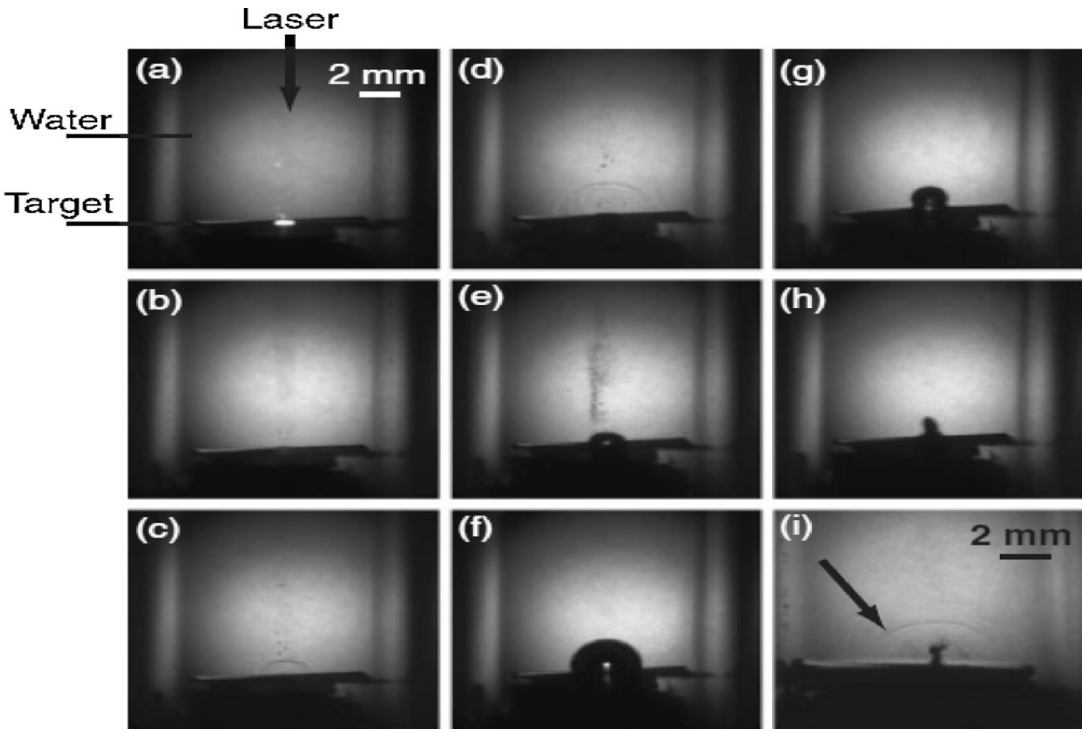

Figure 3-3: The interaction of the laser radiation with matter. [23]

Furthermore, there are number of factors should be taken into account to accomplish the ideal interactions between the laser and materials. For instance, the material state; *solid, liquid or gas;* the material type *insulator, conductor or semiconductor*; the laser beam parameters *pulse width, excitation wavelength, the repetition rate, and beam diameter*. The nature of crystal structure of the solid material in two interfaces experiments *impurities, and defects*; and lastly the relaxation times. [21]

3.4 Advantage and disadvantages of the PLAL technique

"The high power density near the focus of a pulsed laser (>106 W/cm2) allows this method to be applied to nearly all classes of materials." [23] "Laser ablation in non-vacuum environments has benefits due to the reactions in a dense, but temporally short-lived environment. It must be realized that bimolecular (biparticle) bonding in the gas phase requires a third body so as to conserve both momentum and energy." [23]

In contrast to other methods, the high purity of the final products is a highlight of the PLAL technique. Also, PLAL is one of the lowest cost method of the experimental setup compared to other techniques that require a vacuum chamber, high temperature, and high pressure or resource and so on.

To focus more on the advantages of the PLAL technique, there are primary factors that should be kept in mind when thinking about techniques for graphene production. First is the high quality. Second is the control over the crystals' thickness. Third is the mass production for manufacturing demand.

3.5 Methodology to structure Graphene nanoparticles/ Polymer composites

The objective of this research is to fabricate graphene nanoparticles combined with polymer composites. Therefore, three fabrication stages have been applied to each sample to carry out the project's experiments.

3.5.1 First stage

The first stage is the solution preparation by adjusting the weight of the solute. They are (PVA, PMMA, and PS) polymers, and the volume of the appropriate solvents (water, ethanol, and toluene) to insure the most accurate molar solutions before exposing the sonicated mixture. It is worth mentioning that there would be a potential improvement for Toulon analysis if different conditions were fulfilled, but time constraint prevented that since the proposal of this project is quite abroad.

However, the studied solutions in this project are described in Table 3-1.

Table 3-1: The three solutions groups (Water, Ethanol, and Toluene) that have been studied in this project.

Water	Ethanol	Toluene
Pure deionized Water	Pure Ethanol	Pure Toluene
Water+ 0.2% PVA	Ethanol+ 0.2% PMMA	Toluene+ 0.2% PS
Water+ 0.4% PVA	Ethanol+ 0.4% PMMA	Toluene+ 0.4% PS
Water+ 0.6% PVA	Ethanol+ 0.6% PMMA	Toluene+ 0.6% PS
Water+ 0.8% PVA	Ethanol+ 0.8% PMMA	Toluene+ 0.8% PS
Water+ 1% PVA	Ethanol+ 1% PMMA	Toluene+ 1% PS

3.5.2 Seconded stage

The aforementioned solutions with graphite target were exposed for 20 minutes by nanosecond laser. Also, another part of the aforementioned solutions with graphite target was exposed for 20, 60, 90, and 120 minutes by nanosecond laser. A description of the lasers parameters for both kinds used in this project is presented in Table 3-2.

Table 3-2: Laser parameters for both ns- and fs- lasers.

Lasers Specification	Ns-Laser	Fs-laser
Laser type	Neodymium-doped yttrium lithium fluoride (Nd:YLF)	Homemade femtosecond laser
Wavelength	532 nm	800 nm
Pulse width	150 ns	35 fs
Pulse energy	800 μJ	250 μJ
Ablation time	20 min	1-2 hour
Lens focal length	5 cm	5 cm
Repetition rate	1kHz	1kHz
Liquid height	1 cm	1 cm

3.5.3 Third stage

This involved fabricating thin films of GNP achieved by spin coating the different sonicated mixture by basically depositing a few drops of the GNP mixture to the center of a Silicon wafer and applying appropriate speed. Since the main goal is to obtain uniform thin films of graphene, the spin coating procedure is a very basic yet important step for this research, which will result in a much more accurate morphology uniformity as desired while scanning the films surface by either AFM or SEM spectroscopy. After the spin coating comes the thermal annealing procedure, which is the second extremely important factor in fabricating graphene-polymer nanocomposites.

Hence, after a few trials, there were two potential recipes for the graphene's thin films fabrication; whereas the major difference is the baking times "thermal annealing" while the other

parameters are fixed at 90° C annealing temperature and 350 rpm for the spin coater speed for 40 seconds. In other words, a couple of annealing times were performed while fabricating the graphene's thin films until reaching satisfactory results at 30 and 15 minutes annealing times, as Table 3-3 clarifies.

Table 3-3: The two potential recipes for the graphene's thin films fabrication

Recipe #1 (ns-laser)		Recipe #2 (ns-laser) and (fs-laser)	
Spin coating	Baked	Spin coting	Baked
350 rpm	90° C	350 rpm	90° C
40 sec	30 minutes	40 sec	15 minutes

3.6 Conclusion

This chapter covered the history and the principle of the PLAL technique. Also, the experimental setup of the PLAL technique for the reason of growing graphene from a bulk of graphite with the contribution of different polymeric solutions was discussed. Finally, the fabrication process was extensively explained, this involved the two different recipes that carried out in this research to successfully fabricate graphene via the PLAL approach.

Chapter 4: Characterization

4.1 Introduction

The tremendous attention aimed towards developing routes for obtaining high quality and large quantities of graphene has been the focus of a variety of research areas. Therefore, graphene can now be produced by many different approaches. In this work, high quality graphene with controllable thickness was successfully obtained by the PLPA approach from graphite-polymer sources. Various microscopes had been used to examine the investigated products. Therefore, the first central aim of this chapter is to give a concise introduction to Raman spectroscopy and to provide basic information about the most-widely used characterization techniques for GNP analysis, in particular UV-visible, atomic force microscopic (AFM), scanning electron microscope (SEM), and transmission electron microscopy (TEM). The second central aim of this section is to discuss the obtained results.

4.2 Raman Spectroscopy

Raman spectroscopy is considered one of the most efficient non-destructive characterizing techniques used for unraveling the graphene phenomena. The high sensitivity of the Raman spectrum for geometric structure is the major feature for the output accuracy. Analyzing graphene via the Raman spectrum identifies the structure disorder; the purity which is the absence or presence of defect; and most importantly, the number of graphene layers. [26] The Raman spectrum for graphene ideally consists of two essential identification peaks: G band and 2D band as Figure 4-1 shows.

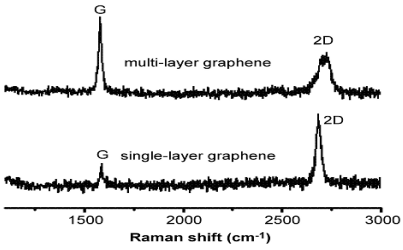

Figure 4-1: Raman multi-layer vs. single-layer spectrum for graphene.

The G and 2D bands commonly exist in the range of ~ 1580 cm^{-1} and ~ 2700 cm^{-1} respectively. [27] Thus; the number of layers can be distinguished by calculating the I_{2D}/I_G ratio as is summarized in Table 4-1.

Table 4-1: Summary of the number of graphene layers by calculating the ratio.

Band	Ratio	Meaning
2D/G	>2-3	Single Layer Graphene
2D/G	Around 1-2	Bilayer Graphene
2D/G	<1	Multilayer Graphene
Width of 2D	Around 25 cm^{-1}	Single Layer Graphene

However; there is a third band designated as D band which could present in the spectrum in the range of 1200-1400 cm^{-1}, where the intensity ratio of D band gives indications regarding the number of defects present in the samples. Furthermore, there is a D' band which can be measured around 1620 cm^{-1} and D+G band referred to as shown in Figure 4-2. [28] [29]

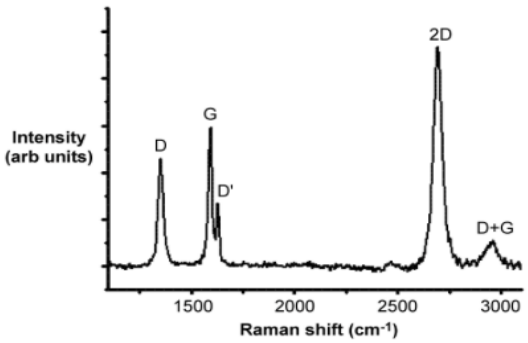

Figure 4-2: Raman identification peaks for grapheme: D-band, G-band, 2D-band, and D+G-band.

Table 4-2 summarizes the average range of graphene fingerprint peaks in the Raman spectrum.

Table 4-2: Summary of the average range of graphene fingerprint peaks in the Raman spectrum.

Name of the band	Scale of Raman shift (cm^{-1})	Representation
D-band	1200-1400	To represent disordered structure of graphene [27]
G-band	1400-1600	To represent modification on the surface of graphene [27]
D'-band	1550-1600	To associate with one elastic and one inelastic scattering event [27]
2D-band	2400-2800	Using to determine the number of layer of graphene [27]
D+G band	2800-3200	To represent that there is no backscattering restriction

4.2.1 Graphene Nanoparticle (GNP): Water/PVA

It's worth to first clarify that most of the following obtained results are very comparable with the previously reported results obtained by *M. Zhang, et al. 2012* as Figure 4-3 shows the pure PVA Raman spectra with the spectrum of the graphene-PVA composite for comparison.

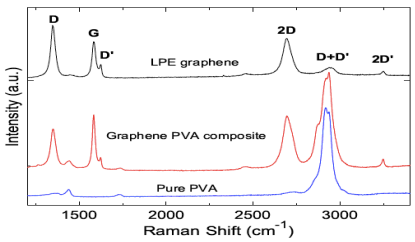

Figure 4-3: Raman spectra of flake on Si/SiO_2, polyvinyl alcohol (PVA), and graphene-PVA composite. [30]

4.2.1.1 Raman analysis Recipe #1 (ns-laser)

Figure 4-4 is the Raman measurements at the room temperature detected by (The Renishaw micro-Raman spectrometer), excitation is accomplished at laser wavelength 488nm, measuring the sample of (water+ graphene+1% PVA) mixture, fabricated on a silicon wafer by the aforementioned Recipe #1 (ns-laser) in the third chapter.

(a)

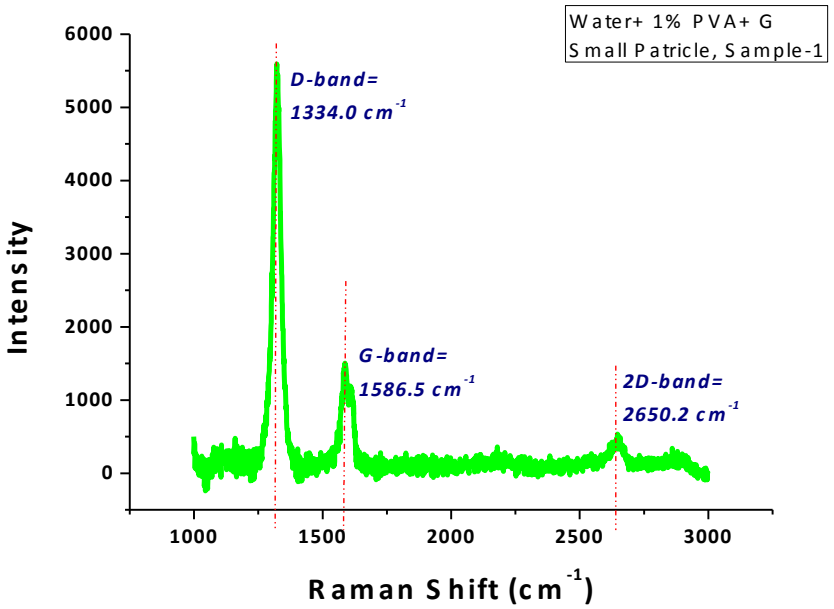

(b)

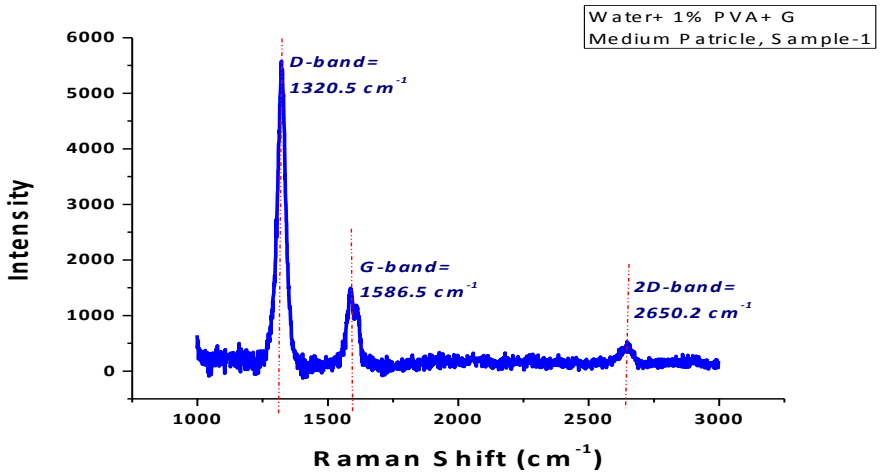

(c) ,(d)

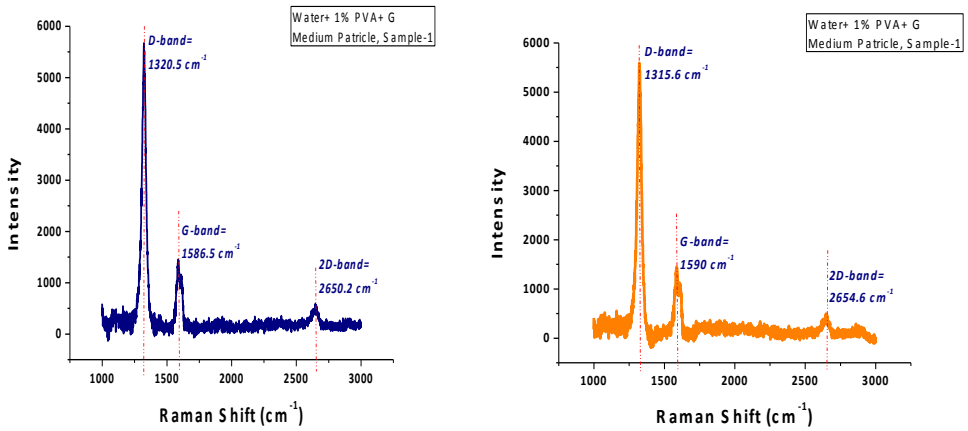

(f)

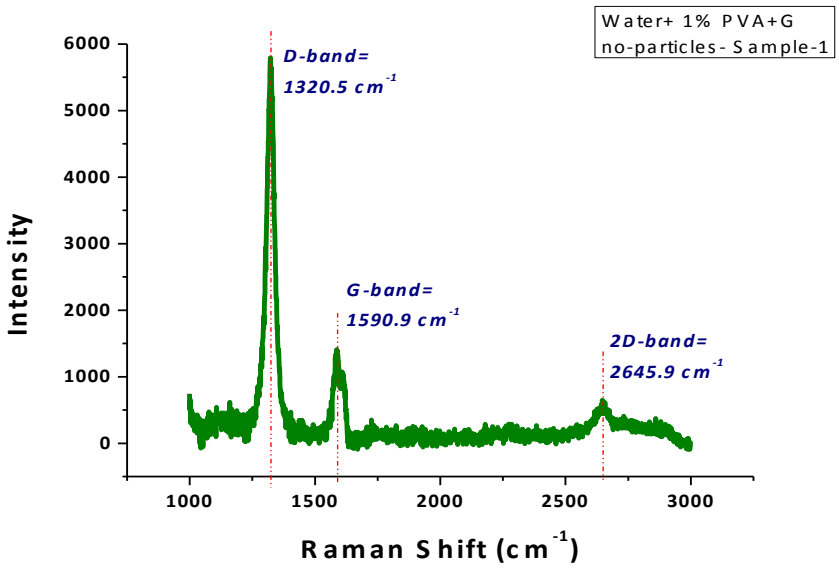

Figure 4-4: Raman spectrum for (water+ 1% PVA+ Graphene) with the laser spot focused on: (a) a small diameter particle, (b)(c)(d) three different medium diameter particles, and f) buffed surface whereas there are smaller dots that can not be seen on the Raman screen.

Spectra a, b, c, d and f were measured on thin films prepared by recipe #1. These spectrums show the most two significant identification peaks of graphene, G and 2D bands, which are clearly visible at (~ 1586 cm^{-1}) and (~ 2650 cm^{-1}) respectively. The present of sharp D-band at (~ 1320 cm^{-1})

indicates a defect on this sample. Yet, Raman spectra of three different medium diameter flakes having the G and 2D peaks at approximately the same intensity are a confirmation for the yields uniformity. Also, Raman spectra showing G and 2D peaks in the default positions of buffed surface, *whereas there are smaller dots that can not be seen on the Raman screen but still detected by the laser*, on the same sample is confirming the products uniformity.

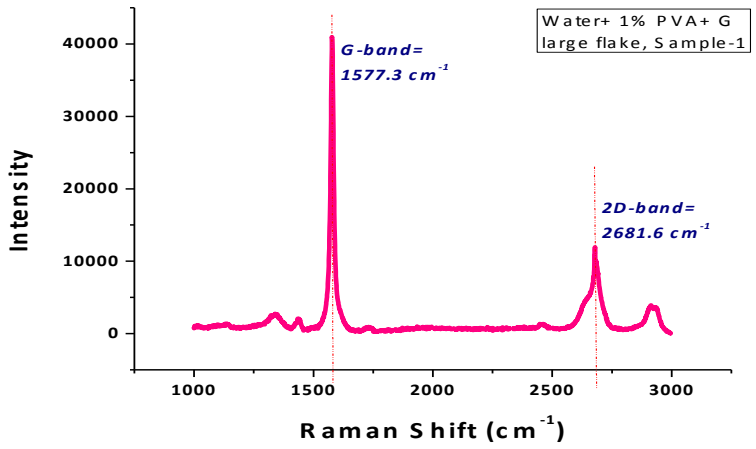

Figure 4-5: Raman spectrum for large diameter flake in a thin film of (water+Graphene+1% PVA)

However, in the above Figure 4-5, when laser is focused on large diameter flake, on the same sample disused above (water+Graphene+1% PVA), a significant improvement in the Raman measurement occurs. The sharp D-band decreased dramatically from (~ 1320 cm^{-1}) in small and medium diameter flakes to very week peak as shown in Figure 4-6.

4.2.1.2 Raman Data for Recipe #2 (ns-laser):

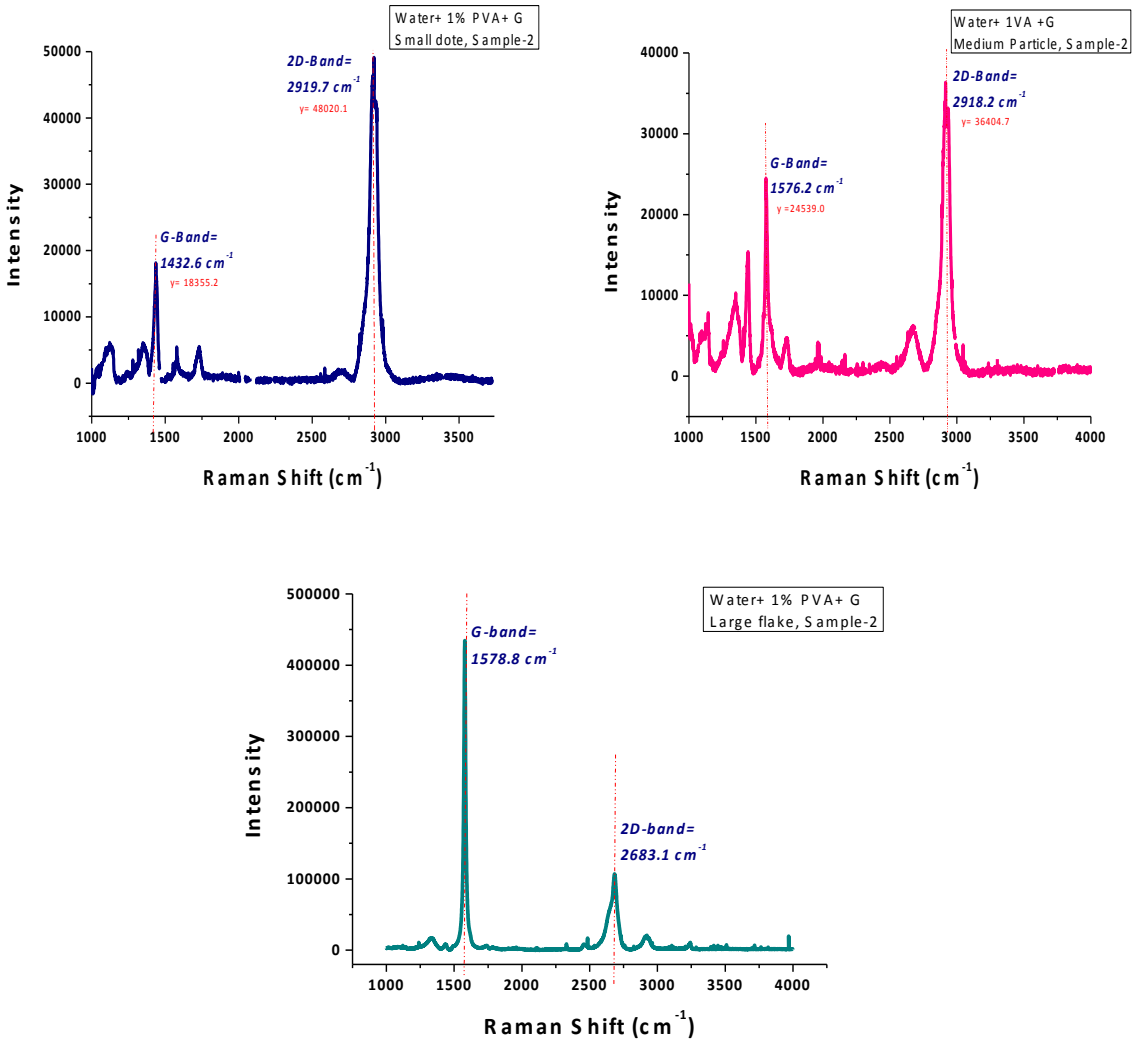

Figure 4-6: Raman spectrum (water+ Graphene+1% PVA) with the laser spot focused on: (a) a small diameter particle, (b) a medium diameter particle, and c) a large diameter flake.

However, in Figure 4-6 the absence of D-band indicating that virtually no defects are present when the laser spot focused for measuring a large diameter flake.

4.2.1.3 Raman Data for Recipe #2 (fs-laser):

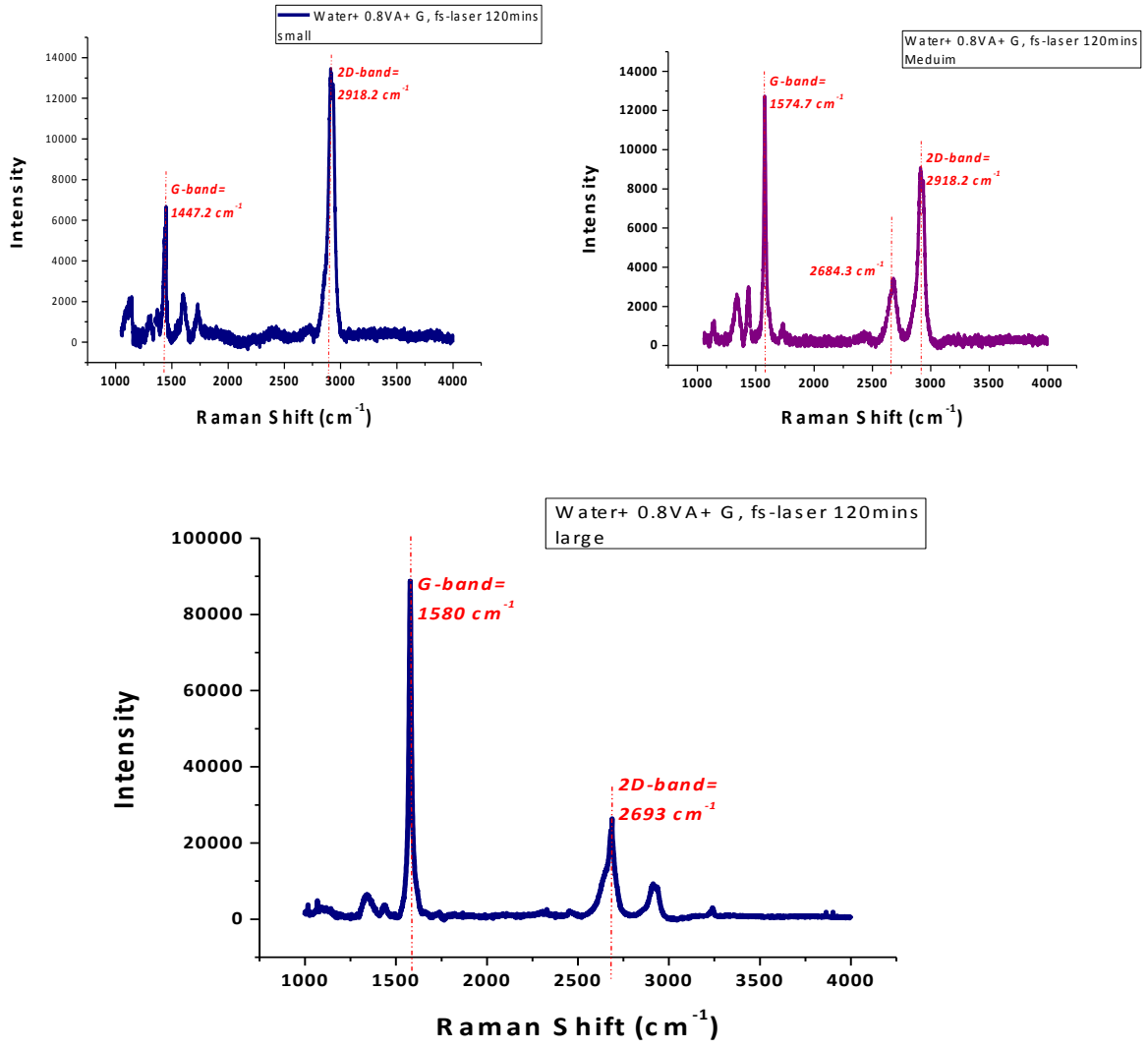

Figure 4-7: Raman spectrum for (water+ Graphene+0.8% PVA) with the laser spot focused on: (a) a small diameter particle, (b) a medium diameter particle, and c) a large diameter flake.

The best Raman measurement in Figure 4-7 in terms of defect free is obtained by increasing the ablation time to 2 hours by femtosecond laser (250-μJ pulse energy) for (water+ Graphene+ 0.8% PVA). The D-band is very week while G and 2D peaks position remaining practically constant and clearly assigned at the expected positions (~ 1580 cm^{-1}) and (~ 2693 cm^{-1}) respectively.

4.2.2 GNP: Ethanol/PMMA

The following Raman spectra in Figure 4-8 present the shape and positions of PMMA-graphene identification peaks. Therefore, it is clearly visible that the Raman shifts for the obtained graphene by PLAL-nanosecond laser consists of similar shape and positions of the G and 2D-bands as the following Figure 4-9 Figure 4-10 Figure 4-11 Figure 4-12 confirm.

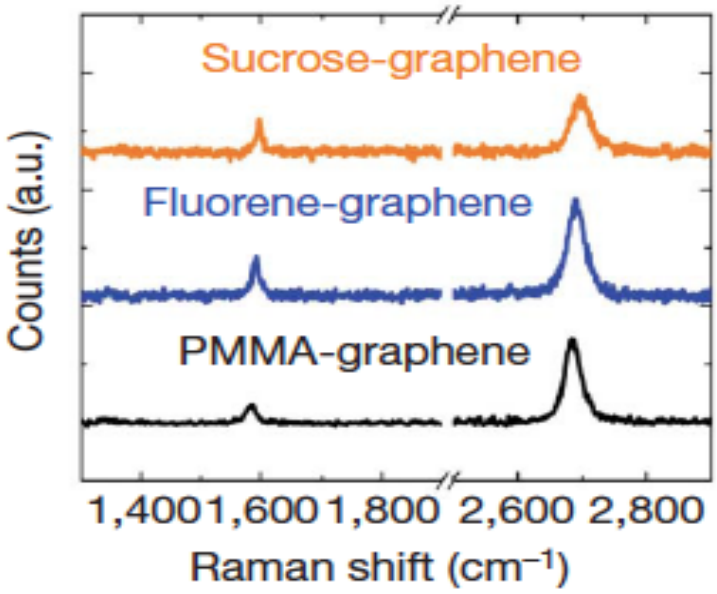

Figure 4-8: Raman spectrum for PMMA-graphene as reported in reference. [22]

4.2.2.1 Raman Data for Recipe #2 (ns-laser):

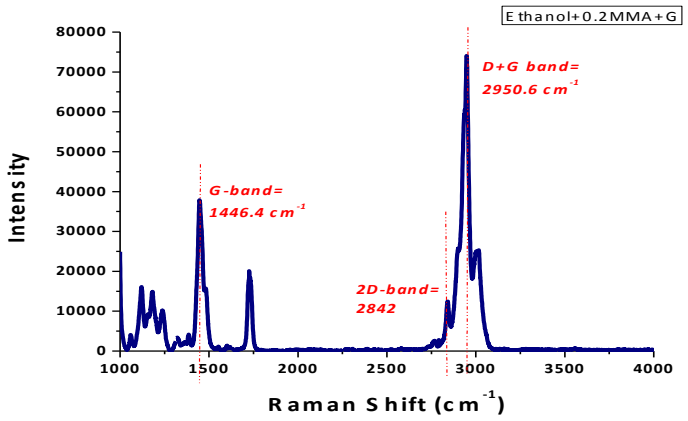

Figure 4-9: **Raman spectrum for ethanol+ 0.2 % PMMA+ Graphene.**

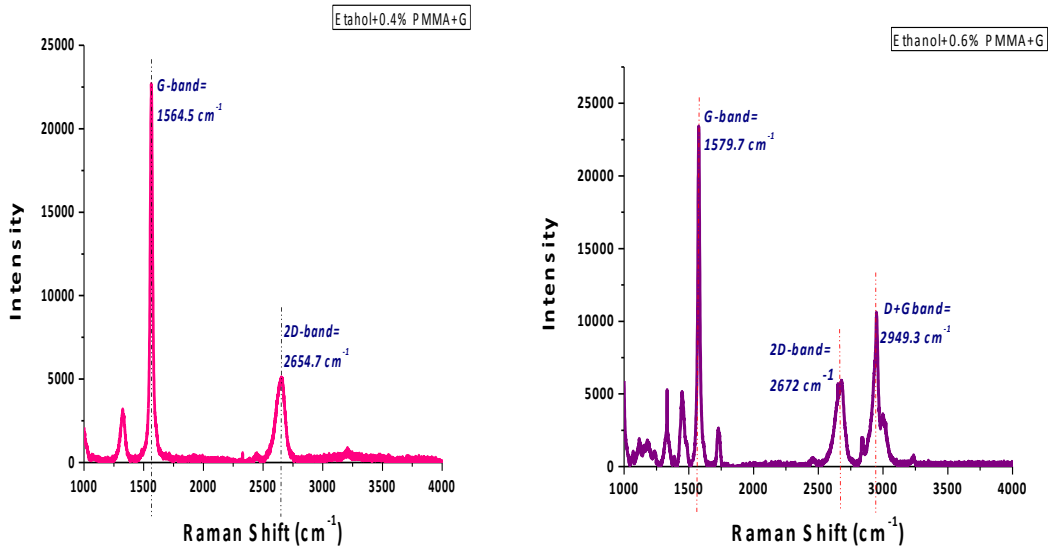

Figure 4-10: Raman spectrum for Ethanol+ 0.4 % PMMA+ Graphene, Ethanol+ 0.6 % PMMA+ Graphene.

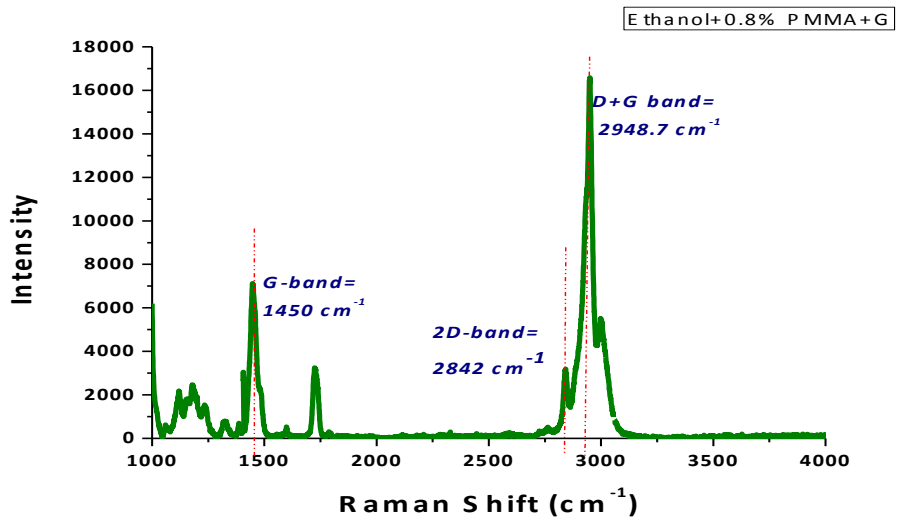

Figure 4-11: Raman spectrum for Ethanol+ 0.8 % PMMA+ Graphene,

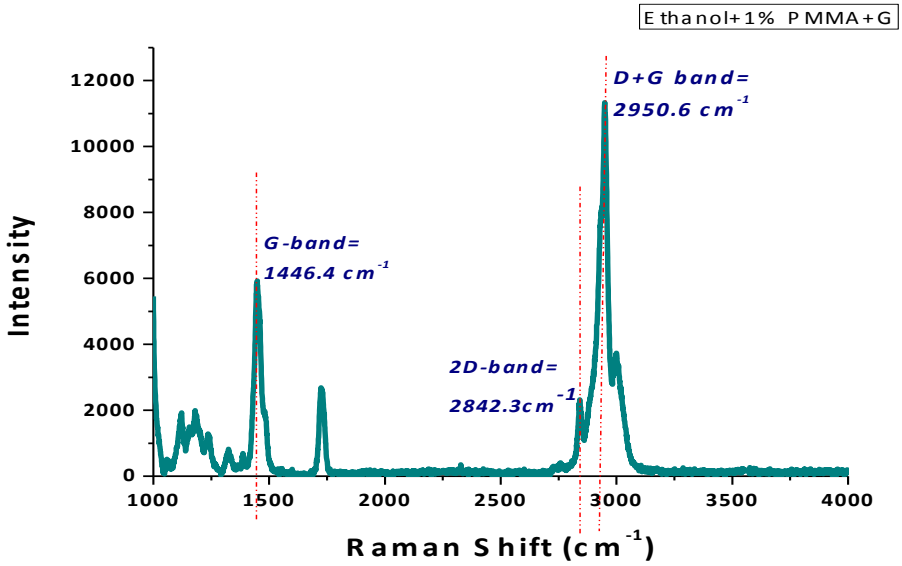

Figure 4-12: Raman spectrum for Ethanol+ 0.8 % PMMA+ Graphene, Ethanol+ 1 % PMMA+ Graphene

4.3 UV-VISIBLE

This system is used to acquire UV-Vis spectra of polymeric graphene solutions with wavelength range from 190-to1100 nm, and 200-to 800 nm, resolutions 0.1 nm, accuracy ±0.3 nm. UV-visible spectra for monolayer and bilayer graphene have a significant peak at 268 nm as Figure 4-13 shows.

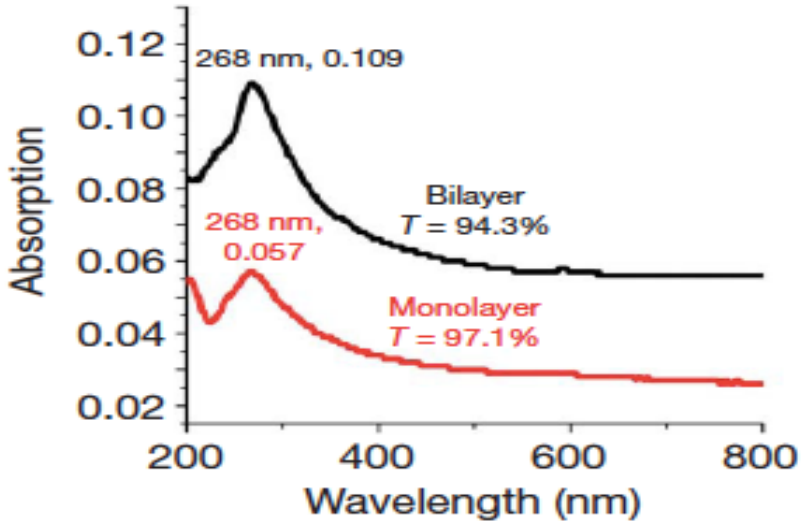

Figure 4-13: UV-VISIBLE absorption spectrum for (a) graphene monolayer- red bottom line, (b) Bilayer graphene black top line, as reported in reference. [22]

4.3.1 GNP: Water/PVA

4.3.1.1 Ns-laser UV-visible data for GNP: Water/PVA:

The following shows the UV-visible in Figure 4-14 is analysis for: first, 20 ml of water as solvent, mixed with different concentrations of PVA polymer 0.2%, 0.4%, 0.6%, 0.8%, and 1% concentration without a graphite sheet employed. Second, is the UV-visible analysis for the aforementioned mixtures exposure for 20 minutes by ns-laser with a power of 800 μJ with a graphite sheet as the graphene source. The diagram below shows the obtained UV-visible absorption spectrum

for GNP: PVA ablated with the aforementioned ns-laser parameters. However, by comparing Figure 4-13 with Figure 4-14, the significant peak at 268 nm wavelength is exit in all different concentration 0.2%, 0.4%, 0.6%, 0.8% and 1% PVA- Polyvinyl alcohol.

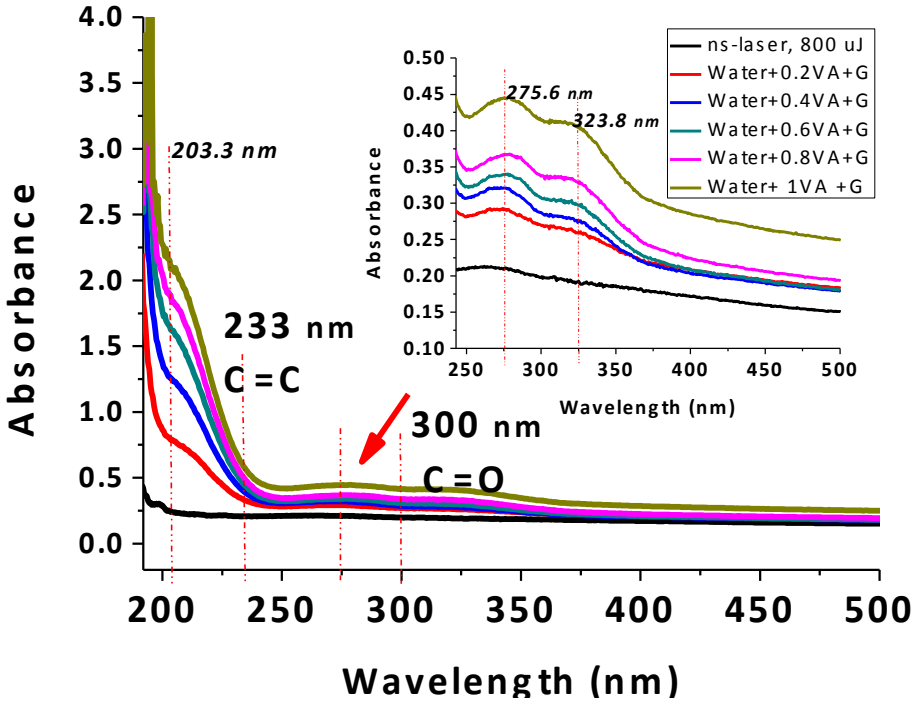

Figure 4-14: The obtained UV-visible absorption spectrum for GNP: Water+ Graphene+ PVA

4.3.1.2 Fs-laser UV-visible data for GNP: Water/PVA:

Herein, the fs-laser effect for 20ml of water as solvent added to 0.8% concentration of PVA mixture is investigated as Figure 4-15 presents, the UV-vis measurement was obtained after exposure four different beakers that were filled with the same amount of 20 ml water, for 20, 60, 90, 120 minutes with the contribution of a graphite sheet

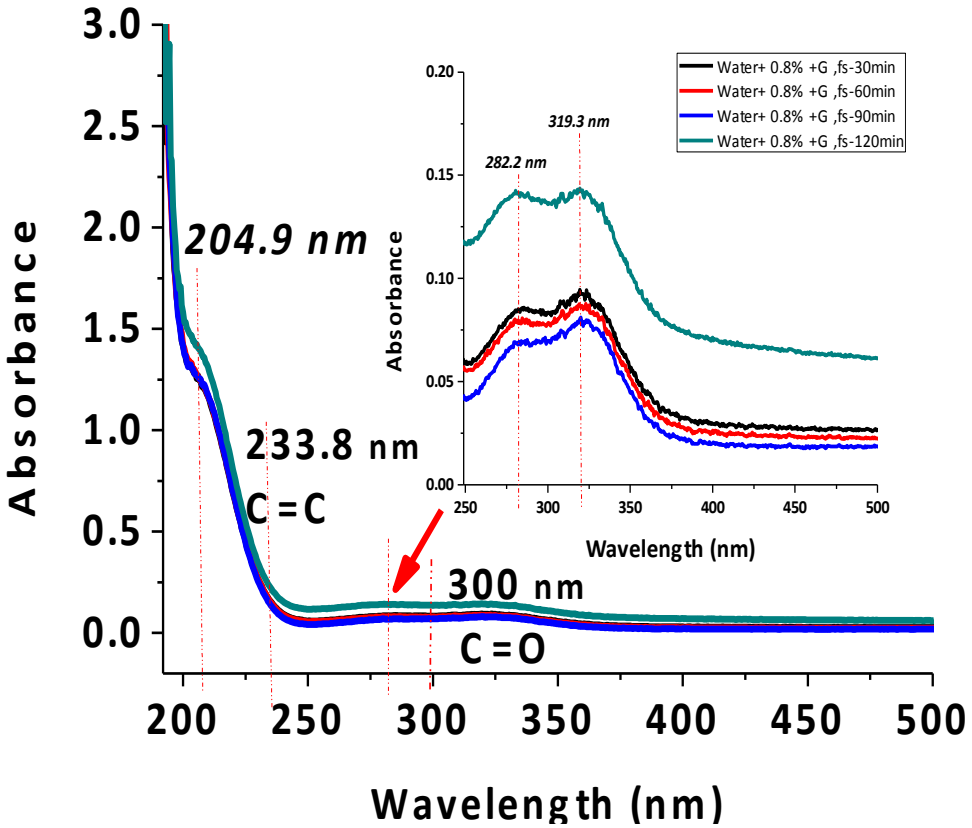

Figure 4-15: The obtained UV-visible absorption spectrum for GNP: Water+ PVA+ Graphene.

4.3.2 GNP: Ethanol/PMMA

The second examined solution is the ethanol added to different concentrations of PMMA-Poly (methyl methacrylate) polymer exposure by aforementioned ns-laser recipe. The black line in Figure 4-16 shows how much is pure PMMA absorbs light when the solution tested with UV-vis spectroscopy which is ~300 nm. Also, the maximum absorbance of pure Ethanol is detected at 237 nm as the dotted arrow in Figure 4-17 shows.

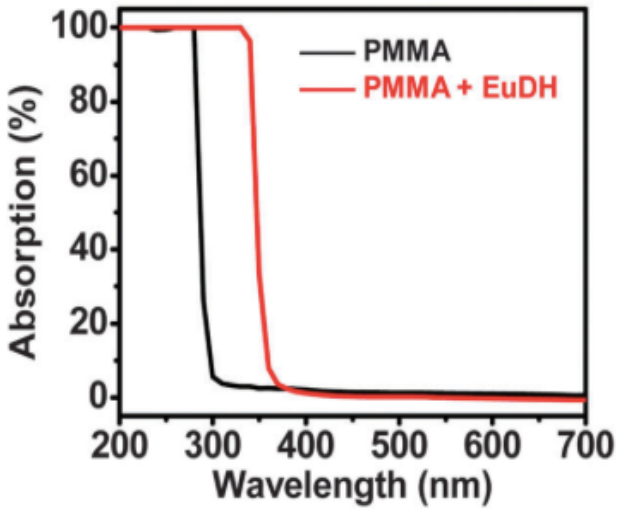

Figure 4-16: The PMMA absorbance- adapted from reference. [31]

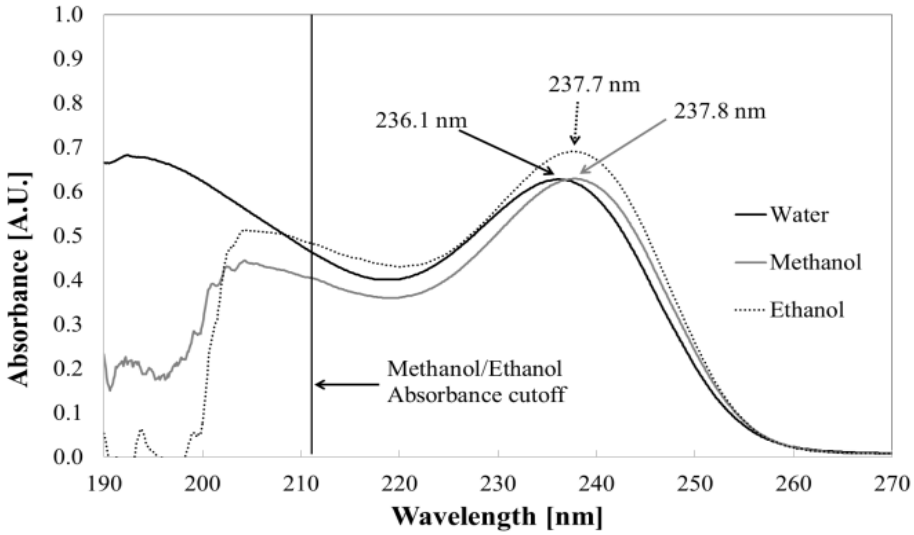

Figure 4-17: The dotted arrow indicates the ethanol absorbance as reported in reference. [32]

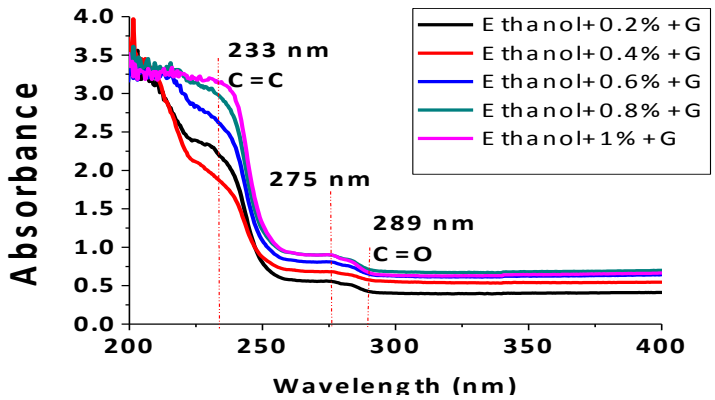

Figure 4-18: The obtained UV-visible absorption spectrum for GNP: ethanol+ PMMA+ Graphene.

In this work, the above Figure 4-18, shows the absorbance of the growing graphene+ PMMA. It has peak at 289 nm (~300 nm) wavelength which represent the pure PMMA absorbance On the other hand; the 233 nm (~237 nm) peak is obviously belongs to the ethanol as reported in Figure 4-17. The graphene absorbance peak should be placed in the area of 268 nm as reported in Figure 4-15. However, Table 4-3 is a simple comparison between the obtained UV-vis spectrum and the spectrum that previously reported in reference. [22], [31], [32] The peak at 275 nm could be the graphene absorbance; more investigation should be taken to confirm the position of this peak.

Table 4-3: UV-vis measurement comparing the obtained spectrum with the reported ones.

Molecule	Maximum absorption (nm), as reported	Maximum absorption(nm), as obtained
Ethanol	237.7 nm	233 nm
PMMA	~300 nm	289
Graphene	268 nm	275 nm

4.4 Surface morphology

Atomic force microscopy and scanning electron microscopy were carried out to analyze the fabricated graphene films surface morphology, thickness, and roughness. Also, transmission electron microscopy was capable of imaging the graphene nanostructure that 20 nm in diameter with significantly high resolution.

4.4.1 AFM

4.4.1.1 (GNP): Water/PVA

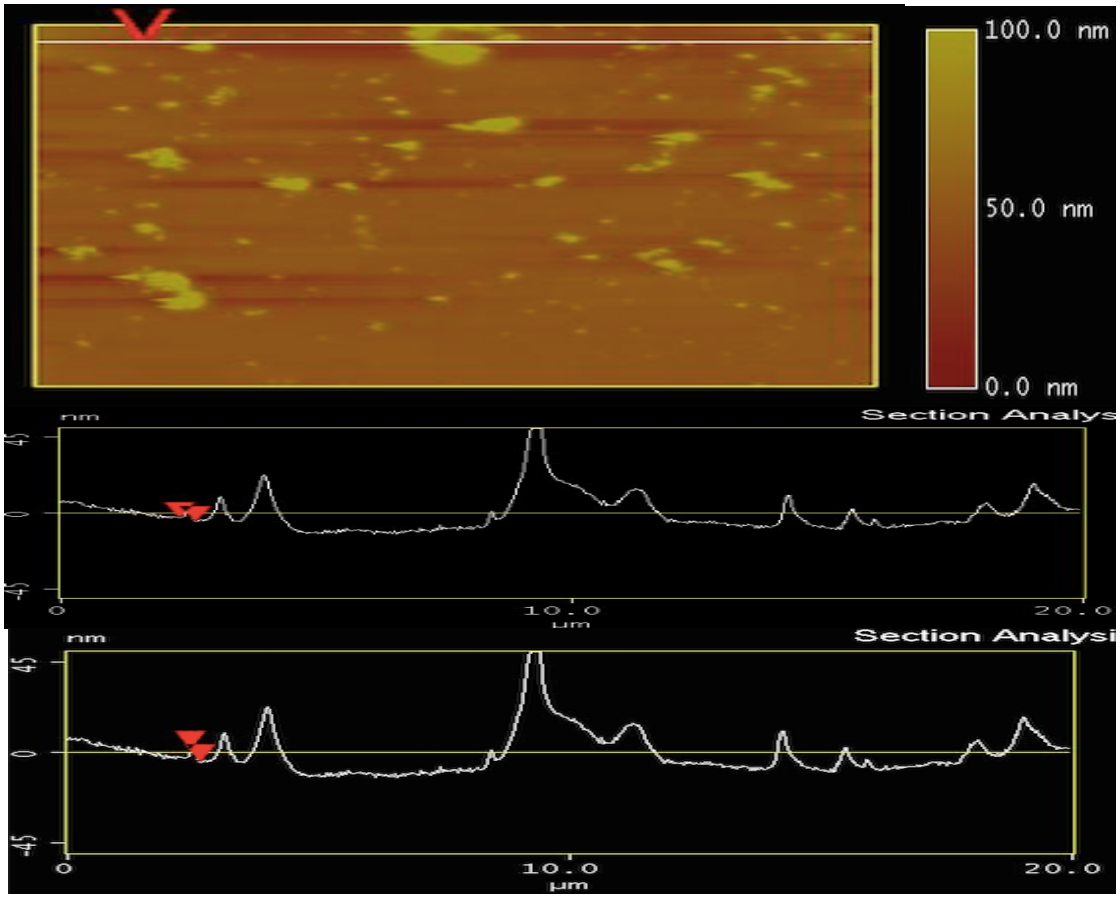

Figure 4-19: AFM images for water+ 1% PVA- ns-laser with Vertical distance = 6.85 nm, and Horizontal distance = 312.5 nm.

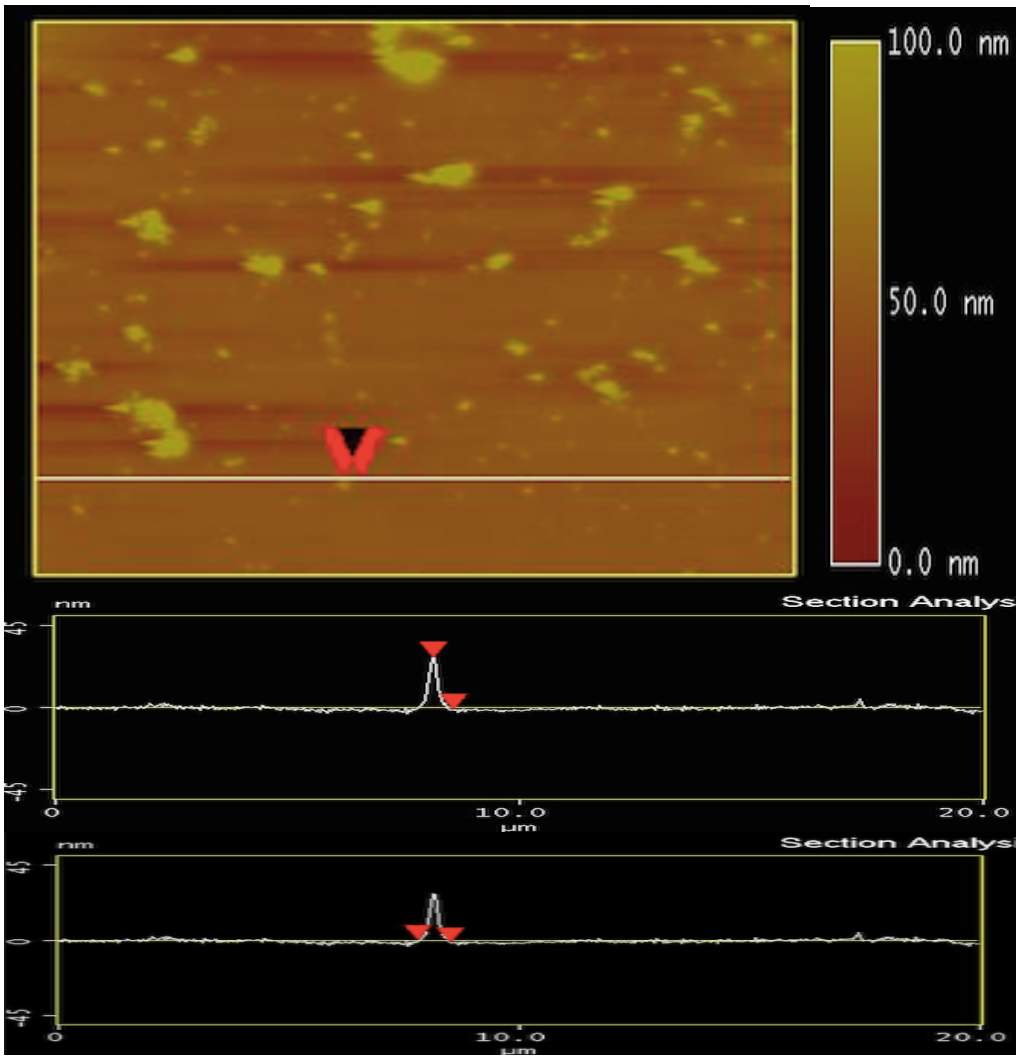

Figure 4-20: AFM images for water+ 1% PVA- ns-laser with Vertical distance = 28.7 nm, and Horizontal distance = 703.1 nm.

4.4.1.2 GNP/ Ethanol + PMMA

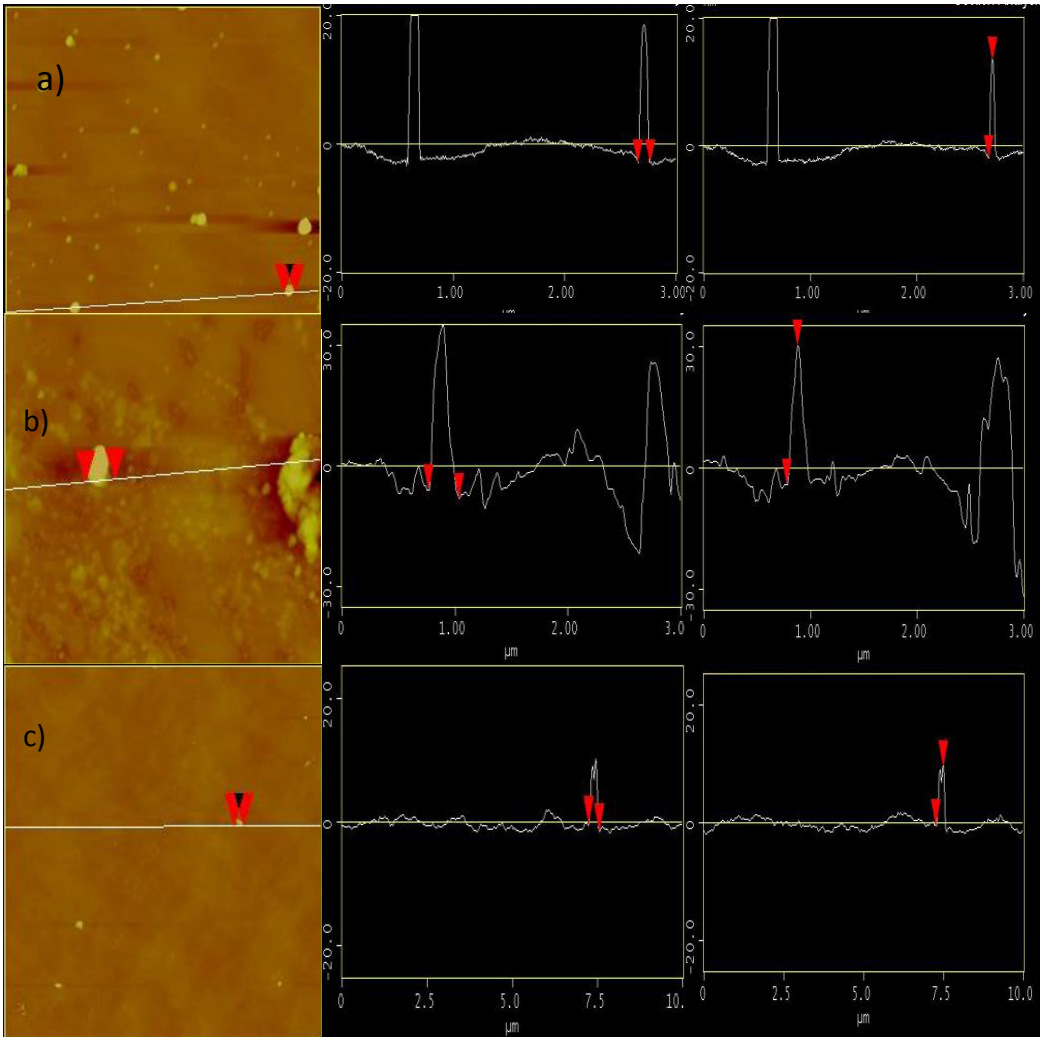

Figure 4-21: AFM images for (a) ethanol, (b) ethanol- 0.2%PMMA (c) ethanol- 0.4%PMMA. The vertical and horizontal distances were measured respectively as (a) 15.4 nm, 111 nm, (b) 34.8 nm, 269 nm, (c) 9.4 nm, 312 nm.

4.4.1.3 (GNP): Toluene/PS

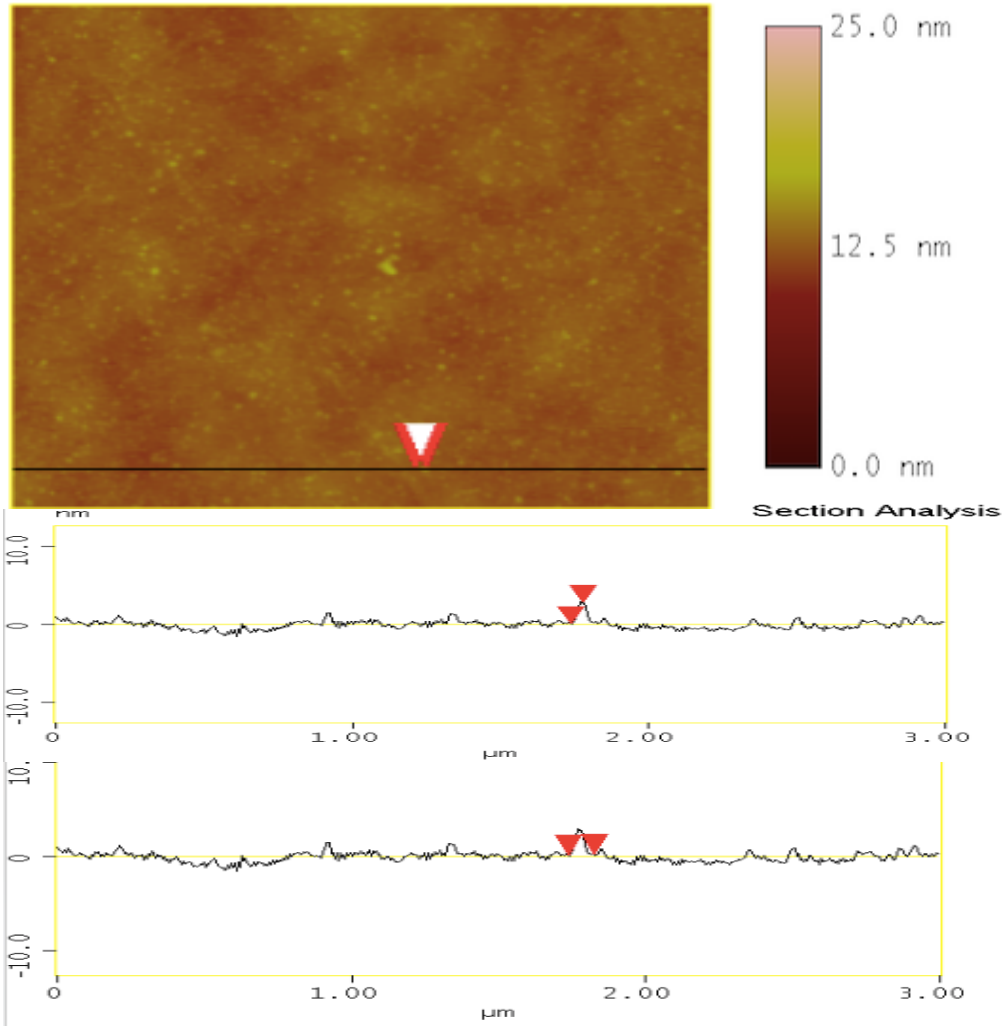

Figure 4-22: AFM images for Toluene- 0.6%PS. The vertical and horizontal distances were measured respectively as 2.78 nm, 87.8 nm.

4.4.2 SEM

Scanning electron microscopy (SEM) is another useful characterization technique to determine the number of graphene layers. Hence, in SEM, there is a liner relationship between the number of graphene layers and the intensity of the secondary electron from the sample operating at low electron accelerating voltage. [26]

4.4.2.1 (GNP): Water/PVA

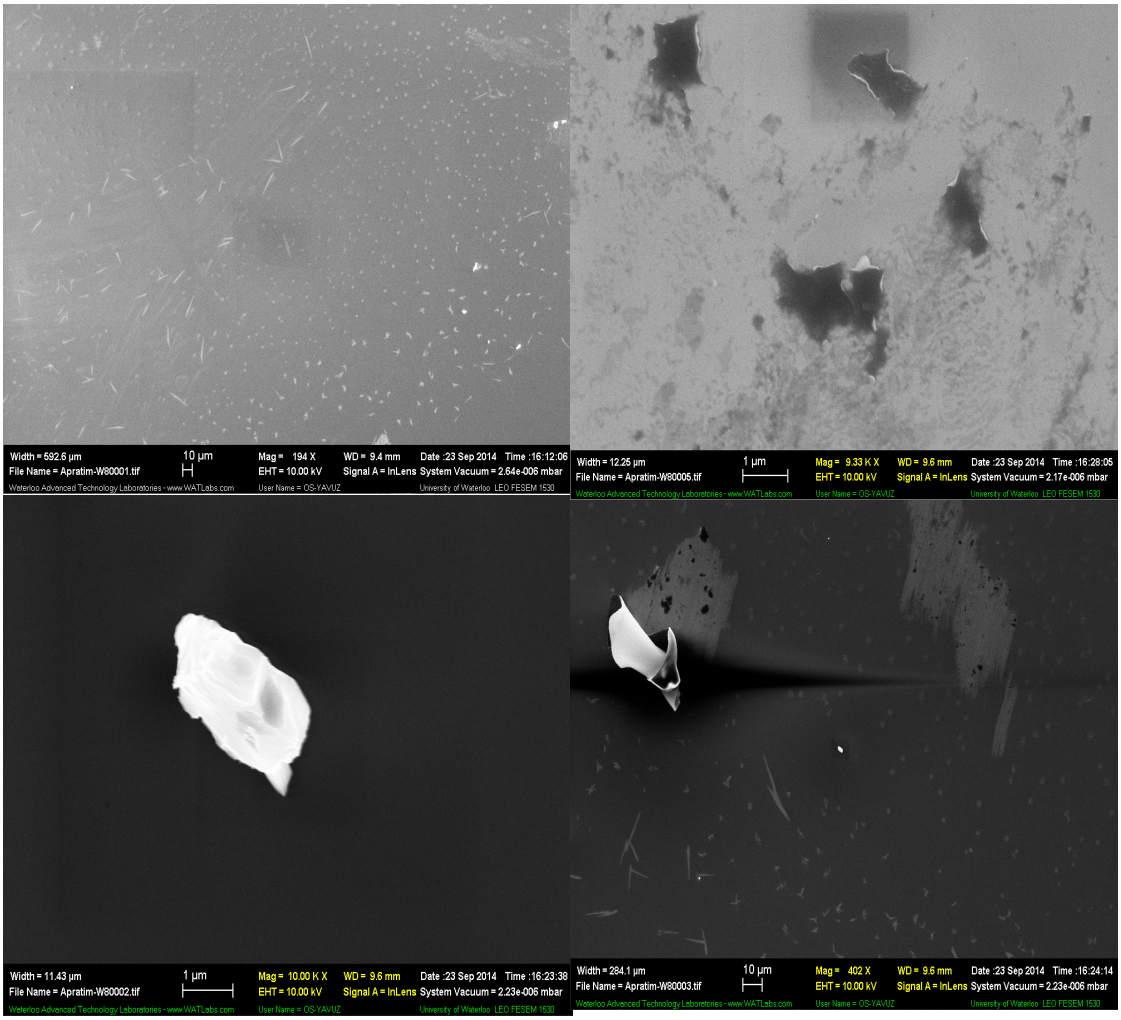

Figure 4-23: SEM images for Water+ graphene.

SEM images estimated the nanoparticles size and show the aggregation level between particles.

4.4.2.2 GNP: Ethanol/PMMA

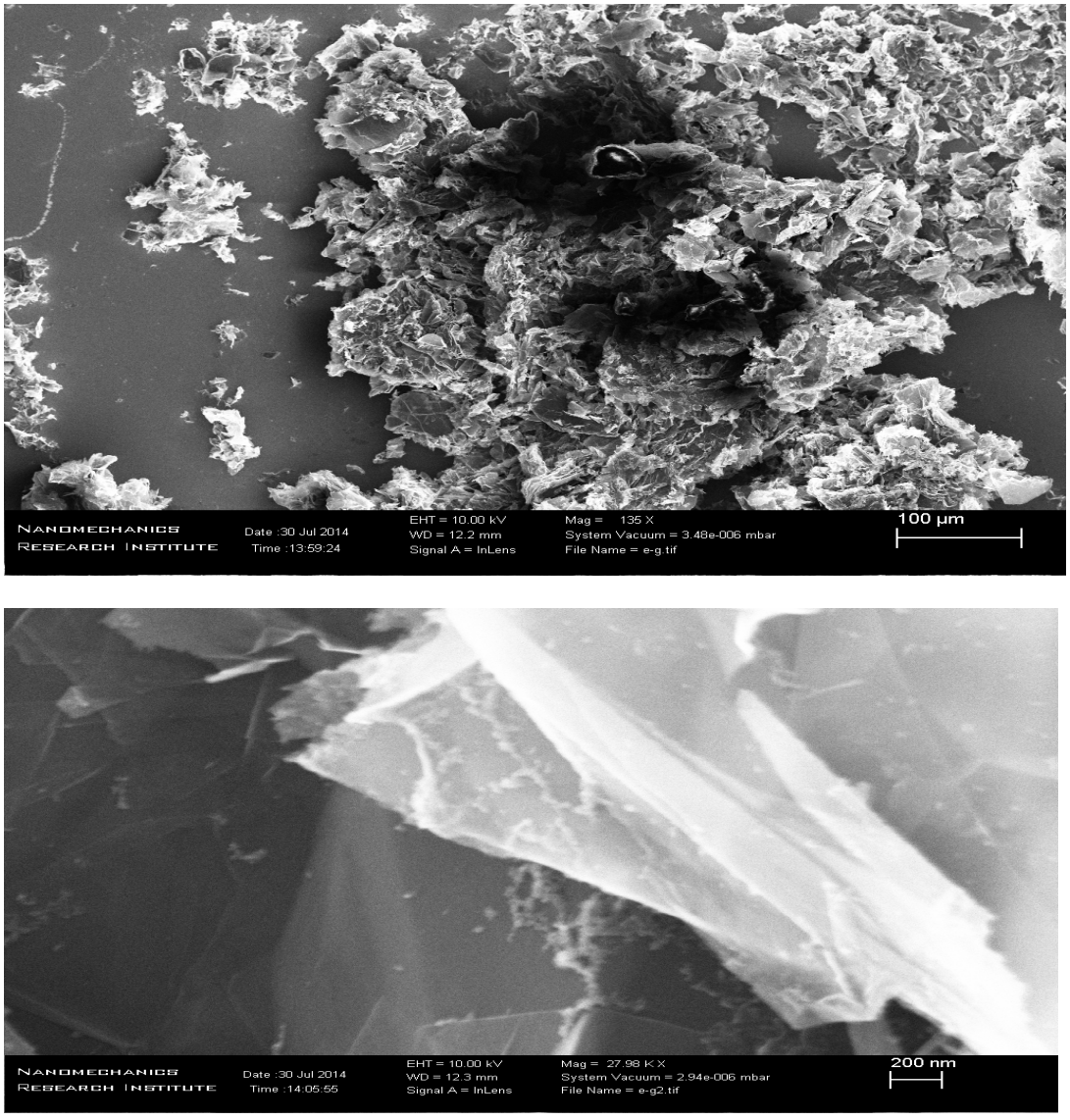

Figure 4-24: SEM images for Ethanol+0.2% PMMA.

Herein, large objects were observed with thickness of more than a few layers. Thus, this is an evidence of a monolayer and few-layer graphene.

4.4.2.3 GNP: Toluene/PS

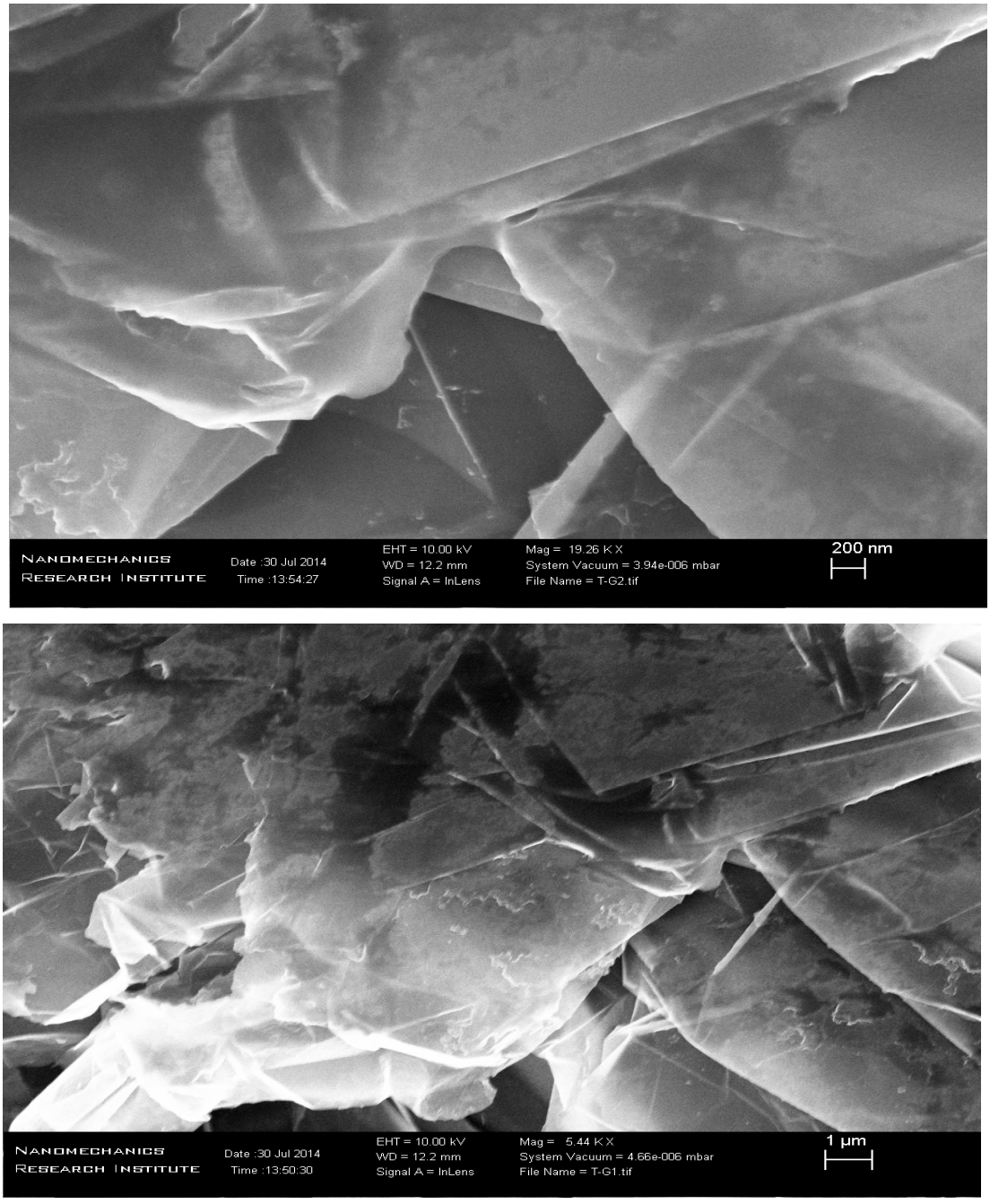

Figure 4-25: SEM images for Toluene 0.2% PS.

4.4.3 TEM

TEM (transmission electron microscopy) is an effective tool highly used to characterize such thin and transparent material. TEM is capable to image individual atoms with resolution less than 1 nm and 20 nm and also can investigate the dispersion state of the material.

4.4.3.1 (GNP): Water/PVA

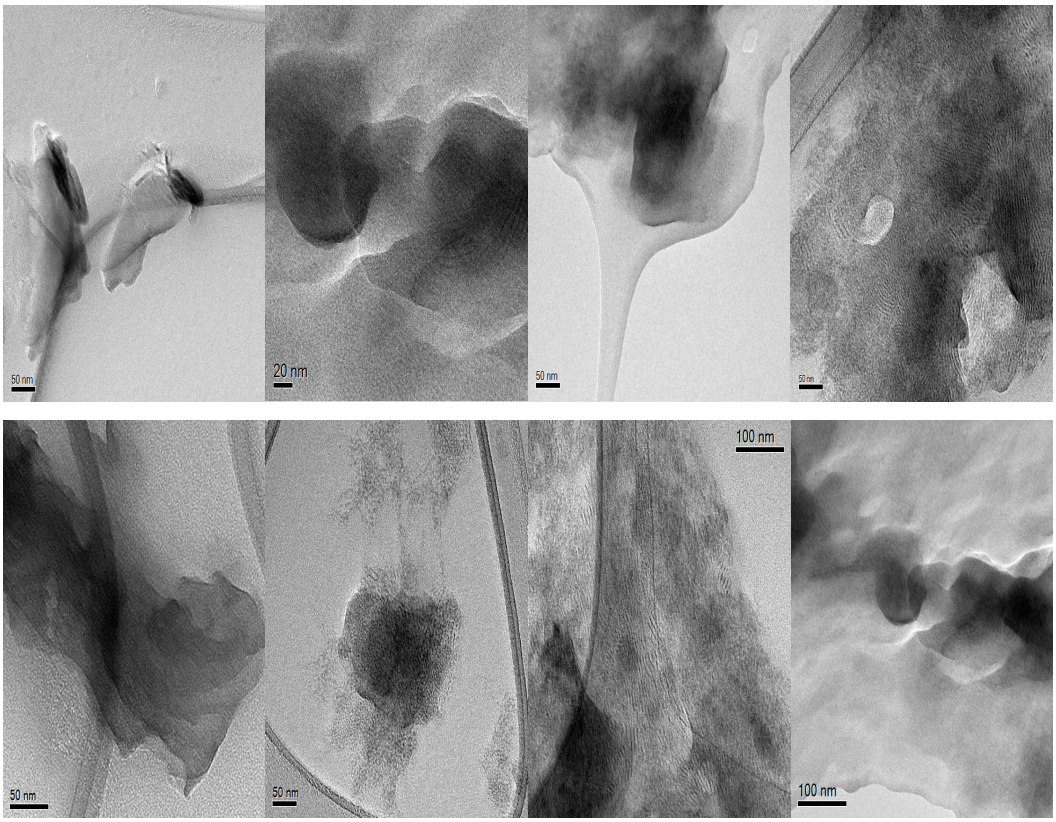

Figure 4-26: TEM images for (Water +graphene+ 1% PVA)- ns-laser, data scale is (50, 20, 50, 50, 50, 50, 100, 100 nm) respectively.

TEM images confirm the function of the polymer for capsules the graphene particles and keep them dispersed.

Chapter 5: Conclusion and Outlook

The outstanding properties of graphene have caused a great sensation since its discovery. Therefore, there has been enormous effort put forth to understand the physical and chemical properties of graphene, followed by establishing several methods experimentally to synthesize single layer and multi layer graphene. The PLAL technique can provide significant changes to the nanostructure-based material, opening new fabrication pathways and generating novel material nano/microstructures.

In this work, a scalable method to produce graphene nanoparticle-polymer composite was investigated. Graphene nanostructure including quantum dots and graphene flakes were also produced. Integrating different types of polymers not only reduced the agglomeration of carbon-based materials but also enhanced the product properties. Finally, fabrication of graphene nanoparticles with purity; controllable particle size; and high uniformity was achieved successfully using the PLAL approach. All characterization techniques and further analysis confirmed that the fabricated graphene thin films consist predominantly of thin graphene particles and flakes with fewer than five layers.

In future work, in terms of a Toluene-PS solution, there is a potential improvement for its analysis if conditions were fulfilled, such as thermal annealing temperature as well as the baking time…etc. Lack of time prevented this, since the scope of the work is quite broad. Also, the obtained GNP should be analyzed by Atomic absorption spectroscopy (AAS) or an alternative technique to determine the concentration of the fabricated polymeric graphene elements. Since AAS can determine different elements in a solution or directly in solid samples; it is an essential analytical technique to precisely measure the amount of outcome products; and, therefore, optimize the recipe for the

manufacturing purposes. On the other hand, analysis of electron diffraction patterns should be considered in future work to give more definitive identification of single and monolayers of graphene.

Bibliography

[1] T. Kuilla, S. Bhadra, D. Yao, N. H. Kim, S. Bose and J. H. Lee, "Recent advances in graphene based polymer composites," *Progress in Polymer Science,* vol. 35, pp. 1350-1375, 2010.

[2] V. Singh, D. Joung, L. Zhai, S. Das, S. I. Khondaker and S. Seal, "Graphene based materials: past, present and future," *Progress in Materials Science,* vol. 56, pp. 1178-1271, 2011.

[3] A. C. Neto, F. Guinea, N. Peres, K. S. Novoselov and A. K. Geim, "The electronic properties of graphene," *Reviews of Modern Physics,* vol. 81, pp. 109, 2009.

[4] G. Eda and M. Chhowalla, "Chemically derived graphene oxide: towards large-area thin-film electronics and optoelectronics," *Adv Mater,* vol. 22, pp. 2392-2415, 2010.

[5] N. Krane, "Preparation of Graphene," *Selected Topics in Physics: Physics of Nanoscale Carbon,* 2011.

[6] W. Ren and H. Cheng, "The global growth of graphene," *Nature Nanotechnology,* vol. 9, pp. 726-730, 2014.

[7] M. J. Allen, V. C. Tung and R. B. Kaner, "Honeycomb carbon: a review of graphene," *Chem. Rev.,* vol. 110, pp. 132-145, 2009.

[8] K. T. Nguyen and Y. Zhao, "Integrated graphene/nanoparticle hybrids for biological and electronic applications," *Nanoscale,* vol. 6, pp. 6245-6266, 2014.

[9] A. Tiwari and M. Syväjärvi, *Graphene Materials: Fundamentals and Emerging Applications.* John Wiley & Sons, 2015.

[10] R. Kumar, A. Sharma, M. Bhatnagar, B. Mehta and S. Rath, "Antireflection properties of graphene layers on planar and textured silicon surfaces," *Nanotechnology,* vol. 24, pp. 165402, 2013.

[11] M. Liu, X. Yin and X. Zhang, "Double-layer graphene optical modulator," *Nano Letters,* vol. 12, pp. 1482-1485, 2012.

[12] F. Schwierz, "Graphene transistors," *Nature Nanotechnology,* vol. 5, pp. 487-496, 2010.

[13] F. Wang, Y. Zhang, C. Tian, C. Girit, A. Zettl, M. Crommie and Y. R. Shen, "Gate-variable optical transitions in graphene," *Science,* vol. 320, pp. 206-209, Apr 11, 2008.

[14] K. T. Nguyen and Y. Zhao, "Integrated graphene/nanoparticle hybrids for biological and electronic applications," *Nanoscale,* vol. 6, pp. 6245-6266, 2014.

[15] S. A. Bashar, "Study of indium tin oxide (ITO) for novel optoelectronic devices," *UMIST, Manchester,* pp. 106-109, 1998.

[16] G. Ouyang, A. Hussain, J. Li and D. Li, "Remarkable permeability enhancement of polyethersulfone (PES) ultrafiltration membrane by blending cobalt oxide/graphene oxide

nanocomposites," *RSC Advances,* vol. 5, pp. 70448-70460, 2015.

[17] H. Huang, Z. Song, N. Wei, L. Shi, Y. Mao, Y. Ying, L. Sun, Z. Xu and X. Peng, "Ultrafast viscous water flow through nanostrand-channelled graphene oxide membranes," *Nature Communications,* vol. 4, 2013..

[18] R. R. Nair, H. A. Wu, P. N. Jayaram, I. V. Grigorieva and A. K. Geim, "Unimpeded permeation of water through helium-leak-tight graphene-based membranes," *Science,* vol. 335, pp. 442-444, Jan 27, 2012.

[19] G. Alexander I. (). *nanostructured material* ["Glossary" online]. Available: http://eng.thesaurus.rusnano.com/wiki/article1371.

[20] A. Z. Alzahrani, *Structural and Electronic Properties of Graphene upon Molecular Adsorption: DFT Comparative Analysis.* INTECH Open Access Publisher, 2011.

[21] R. Nikov, N. Nedyalkov, A. Nikolov, P. Atanasov, M. Alexandrov and D. Karashanova, "Formation of bimetallic nanoparticles by pulsed laser ablation of multicomponent thin films in water," in *Eighteenth International School on Quantum Electronics: Laser Physics and Applications,* 2015, pp. 94470M-94470M-7.

[22] K. Habiba, V. I. Makarov, B. R. Weiner and G. Morell, "Fabrication of Nanomaterials by Pulsed Laser Synthesis,"

[23] Z. Sun, Z. Yan, J. Yao, E. Beitler, Y. Zhu and J. M. Tour, "Growth of graphene from solid carbon sources," *Nature,* vol. 468, pp. 549-552, 2010.

[24] Z. Yan and D. B. Chrisey, "Pulsed laser ablation in liquid for micro-/nanostructure generation," *Journal of Photochemistry and Photobiology C: Photochemistry Reviews,* vol. 13, pp. 204-223, 2012.

[25] G. Ledoux, D. Amans, C. Dujardin and K. Masenelli-Varlot, "Facile and rapid synthesis of highly luminescent nanoparticles via pulsed laser ablation in liquid," *Nanotechnology,* vol. 20, pp. 445605, 2009.

[26] H. A. VURAL, *Synthesization of Noble Metal Nanoparticles by Pulsed Laser Ablation Method in Liquids and Thin Film Applications,* 2012.

[27] C. N. R. Rao and A. K. Sood, *Graphene: Synthesis, Properties, and Phenomena.* John Wiley & Sons, 2013.

[28] A. C. Ferrari, "Raman spectroscopy of graphene and graphite: disorder, electron–phonon coupling, doping and nonadiabatic effects," *Solid State Commun.,* vol. 143, pp. 47-57, 2007.

[29] A. Kaniyoor, T. T. Baby and S. Ramaprabhu, "Graphene synthesis via hydrogen induced low temperature exfoliation of graphite oxide," *Journal of Materials Chemistry,* vol. 20, pp. 8467-8469, 2010.

[30] M. Wall, "The Raman Spectroscopy of Graphene and the Determination of Layer Thickness," 2011.

[31] M. Zhang, E. Kelleher, F. Torrisi, Z. Sun, T. Hasan, D. Popa, F. Wang, A. Ferrari, S. Popov and J. Taylor, "Tm-doped fiber laser mode-locked by graphene-polymer composite," *Optics Express,* vol. 20, pp. 25077-25084, 2012.

[32] X. Sheng, C. J. Corcoran, J. He, L. Shen, S. Kim, J. Park, R. G. Nuzzo and J. A. Rogers, "Enhanced ultraviolet responses in thin-film InGaP solar cells by down-shifting," *Phys.Chem.Chem.Phys.,* vol. 15, pp. 20434-20437, 2013.

[33] G. F. De Paula, G. I. Netto and L. H. C. Mattoso, "Physical and chemical characterization of poly (hexamethylene biguanide) hydrochloride," *Polymers,* vol. 3, pp. 928-941, 2011.